

Simulating the thermochemical magmatic and tectonic evolution of Venus's mantle and lithosphere: Two-dimensional models

Marina Armann¹ and Paul J. Tackley¹

Received 5 August 2012; revised 11 October 2012; accepted 17 October 2012; published 13 December 2012.

[1] Numerical convection models of the thermochemical evolution of Venus are compared to present-day topography and geoid and recent resurfacing history. The models include melting, magmatism, decaying heat-producing elements, core cooling, realistic temperature-dependent viscosity and either stagnant lid or episodic lithospheric overturn. In stagnant lid convection the dominant mode of heat loss is magmatic heat pipe, which requires massive magmatism and produces very thick crust, inconsistent with observations. Partitioning of heat-producing elements into the crust helps but does not help enough. Episodic lid overturn interspersed by periods of quiescence effectively loses Venus's heat while giving lower rates of volcanism and a thinner crust. Calculations predict 5–8 overturn events over Venus's history, each lasting ~ 150 Myr, initiating in one place and then spreading globally. During quiescent periods convection keeps the lithosphere thin. Magmatism keeps the mantle temperature \sim constant over Venus's history. Crustal recycling occurs by entrainment in stagnant lid convection, and by lid overturn in episodic mode. Venus-like amplitudes of topography and geoid can be produced in either stagnant or episodic modes, with a viscosity profile that is Earth-like but shifted to higher values. The basalt density inversion below the olivine-perovskite transition causes compositional stratification around 730 km; breakdown of this layering increases episodicity but far less than episodic lid overturn. The classical stagnant lid mode with interior temperature \sim rheological temperature scale lower than T_{CMB} is not reached because mantle temperature is controlled by magmatism while the core cools slowly from a superheated start. Core heat flow decreases with time, possibly shutting off the dynamo, particularly in episodic cases.

Citation: Armann, M., and P. J. Tackley (2012), Simulating the thermochemical magmatic and tectonic evolution of Venus's mantle and lithosphere: Two-dimensional models, *J. Geophys. Res.*, 117, E12003, doi:10.1029/2012JE004231.

1. Introduction

[2] Several first-order aspects of the dynamics of Venus's mantle remain poorly understood, including how the mantle loses its radiogenic heat, the related question of whether its long-term evolution is episodic (e.g., with global resurfacing events) or continuous, the thickness of the lithosphere and crust, and the interpretation of geoid and topography in terms of internal structure. These various points are now reviewed, together with previous numerical models of Venus.

1.1. Heat Loss: Continuous Versus Episodic

[3] The most fundamental question is how Venus's mantle loses its radiogenic heat if, as seems likely, it has a comparable

concentration of heat-producing elements to Earth [Namiki and Solomon, 1998; Turcotte, 1995]. Conduction through a stagnant lithosphere is too inefficient: Reese *et al.* [1998] find that the maximum heat transfer possible without widespread melting is 20 mW/m^2 . If widespread melting occurs then a magmatic "heat pipe" mechanism, as is commonly thought to transport most of Io's tidally generated heat through its lithosphere [Carr *et al.*, 1998; Moore, 2001; O'Reilly and Davies, 1981; Stevenson and McNamara, 1988], is an obvious possibility, and has been considered in some parameterized models of Venus [Spohn, 1991; van Thienen *et al.*, 2005]. Another possibility is that Venus had some type of plate tectonics; either episodic overturn of the lithosphere [Turcotte, 1993, 1995], or plate tectonics that subsequently froze [Solomatov and Moresi, 1996]. Indeed, some features on Venus have been identified as possible subduction zones [McKenzie *et al.*, 1992; Sandwell and Schubert, 1992a, 1992b; Schubert and Sandwell, 1995] or spreading centers [Stoddard and Jurdy, 2012].

[4] Concentrating most of Venus's inventory of heat-producing elements into the crust has also been proposed, although Turcotte [1995] considered it highly unlikely because of the

¹Institute of Geophysics, Department of Earth Sciences, ETH Zurich, Zurich, Switzerland.

Corresponding author: P. J. Tackley, Institute of Geophysics, Department of Earth Sciences, ETH Zurich, Sonneggstrasse 5, CH-8092 Zurich, Switzerland. (ptackley@ethz.ch)

high crustal temperatures that would result and the measured concentrations of heat-producing elements. Measurements by the Vega and Venera landers of heat-producing element concentrations in Venus's crust are summarized in *Turcotte* [1995, Table 2]. The heat production rate H of the samples is intermediate between E-MORB and OIB on Earth: relative to a plausible bulk silicate Earth heat production rate $H_{\text{BSE}} = 5.2 \times 10^{-12}$ W/kg, four samples range between 14 and 33 H_{BSE} , with one outlier at 102 H_{BSE} .

[5] An episodic resurfacing scenario is consistent with the inference from crater counting of a relatively uniform surface age of 300–700 Ma [*Herrick*, 1994; *Schaber et al.*, 1992; *Strom et al.*, 1994], although the crater distribution could instead be explained by an equilibrium “random resurfacing” model [*Bjonnes et al.*, 2012; *Hauck et al.*, 1998; *Phillips et al.*, 1992]. Also, *Brown and Grimm* [1999] argue that the lithospheric thickness required by surface features implies monotonic thickening over the recorded history, although such a monotonic history is questioned by *Guest and Stofan* [1999].

[6] It is instructive to estimate the magmatic resurfacing rate necessary to transport Venus's internal heat to the surface. Magmatism releases heat in two ways: latent heat, and rapid cooling from the interior temperature to the surface temperature (see discussion in *Nakagawa and Tackley* [2012]). Assuming an internal heating rate similar to Earth's of 5×10^{-12} W/kg [*Sun and McDonough*, 1989], a mantle mass of 3.3×10^{24} kg, latent heat of 500 kJ/mol, specific heat capacity of 1000 J/kg/K, temperature drop from melting region to surface of 500 K, and a basalt density of 3000 kg/m³ yields an estimate of 173.6 km³/yr of new crust (consistent with the early estimate of *Solomon and Head* [1982]). This is an order of magnitude more than produced at spreading centers on Earth (about 20 km³/yr, based on 2.9 km²/yr area of new oceanic floor [*Phipps Morgan*, 1998] multiplied by an average thickness of 7 km). Furthermore, this produces crust of thickness 300 m/Ma or 300 km/Ga; such that if the mean crustal thickness is 60 km this would require replacing the entire crust every 200 Myr. Such voluminous magmatism, an order of magnitude higher than Earth's and requiring replacing the entire crust every 200 Myr, appears to be inconsistent with the 300–700 Ma surface age inferred for Venus. Even though active hot spot volcanism was recently claimed on Venus [*Smrekar et al.*, 2010], the estimated magmatic rate is only consistent with the 1 km³/yr equilibrium resurfacing end-member model of *Phillips et al.* [1992]. A larger estimate comes from the outgassing rate needed to give the current SO₂ levels in the clouds: 0.3–11 km³/yr according to *Fegley and Prinn* [1989] or 4.6 to 9.2 km³/yr by *Bullock and Grinspoon* [2001].

1.2. Surface Features

[7] There have been various interpretations of surface features in terms of mantle upwellings or downwellings. On Earth, the highest regions are caused by continental collision above mantle downwellings (slabs), and a similar interpretation of broad plateau-shaped highlands such as Ishtar Terra, Alpha Regio, Thetis Regio, as being above regions of convergence and downwelling has also been advanced for Venus [*Bindschadler et al.*, 1990, 1992; *Buck*, 1992; *Kiefer and Hager*, 1991a, 1991b; *Lenardic et al.*, 1991, 1993, 1995]. More localized rises with volcanism such as Beta, Bell and

Atla Regios are generally interpreted to be caused by mantle plumes [*Basilevsky and Head*, 2007; *Bindschadler et al.*, 1992; *Nimmo and McKenzie*, 1996; *Smrekar and Parmentier*, 1996; *Stofan et al.*, 1995].

[8] Various mechanisms have been proposed to cause coronae, including transient upwelling plumes [*Dombard et al.*, 2007; *Johnson and Richards*, 2003], diapirs [*Janes et al.*, 1992; *Koch and Manga*, 1996; *Stofan et al.*, 1991], breakup of a large-scale plume [*Smrekar and Stofan*, 1999], pervasive small-scale upwellings [*Herrick*, 1999] and gravitational Rayleigh-Taylor instability of the lithosphere [*Hoogenboom and Houseman*, 2006].

[9] Surface deformation strain rates of 10^{-17} – 10^{-18} /s are inferred for recent history and up to 10^{-15} /s in the past when tessera were formed [*Grimm*, 1994a], indicating that the term “stagnant lid” is more accurate than “rigid lid” to describe the tectonic mode [e.g., *Solomatov and Moresi*, 1996].

1.3. Crustal Thickness

[10] The main constraint on crustal thickness comes from interpreting gravity (typically geoid) and topography in terms of isostatically supported variations in crustal thickness. *Konopliv and Sjogren* [1994], in a global analysis of geoid and topography, found that spherical harmonics in the range 30–60 are well matched by Airy isostasy with a depth of compensation (moho depth) of 25–50 km. *Simons et al.* [1994], using a regional spectral approach, found that the apparent depth of compensation (ADC) for spherical harmonics around 50 varies from 25 to 50 km depending on area. *Grimm* [1994b] calculated ADCs for plateau-like highlands of 20–40 km, while *Kucinskas and Turcotte* [1994] obtained estimates of 50–60 km for Ovda and Thetis, using a spatial analysis.

1.4. Geoid and Topography

[11] On Venus, unlike on Earth, a strong positive correlation between geoid and topography is observed. At long wavelengths admittance ratios are high, leading to the inference of a large depth of compensation, which is commonly taken to represent the thickness of the lithosphere. Such an interpretation leads to large values for the thickness of Venus's lithosphere, i.e., 150–250 km, much larger than expected for quasi steady state convection with a similar heat flux to that of the Earth [*Turcotte*, 1993]. For a detailed review of the constraints and interpretations see *Wieczorek* [2007].

[12] There have been different hypotheses for what causes the observed admittance ratios, both in general and from one region to another. At long wavelengths, geoid and topography are expected to be unaffected by elasticity [*Pauer et al.*, 2006; *Steinberger et al.*, 2010], although a recent modeling study [*Golle et al.*, 2012] questions this. Some authors have modeled long wavelength geoid and topography in terms of convection-related density anomalies below a constant-thickness lithosphere, either for plumes [e.g., *Kiefer and Hager*, 1992; *McKenzie*, 1994] or in general [*Pauer et al.*, 2006; *Steinberger et al.*, 2010]. In limited regions, variations in crustal thickness may be the dominant cause [*McKenzie*, 1994; *Simons et al.*, 1997]. The recent study of *Orth and Solomatov* [2011] finds, however, that in stagnant lid convection geoid and topography are caused, to first order, by isostatically supported variations in lid thickness associated with convection rather than deeper density anomalies or “tractions at the base of the lithosphere.”

supporting earlier inferences made of individual features [Moore and Schubert, 1995; Moore and Schubert, 1997; Vezolainen et al., 2003]. Curiously, earlier convection models that were not in the stagnant lid mode did obtain Venus-like geoid and topography ratios even with a relatively thin top thermal boundary layer [Moresi and Parsons, 1995; Schubert et al., 1997], but the differing structure of convection makes these not directly applicable to Venus.

1.5. Global Mantle Convection Models

[13] Several authors have applied purely thermal global convection models to Venus. For isoviscous 3-D spherical models Schubert et al. [1990] found that a rigid outer boundary condition produces more numerous plumes and less coherent downwellings than a free-slip outer boundary condition. Increasing the viscosity contrast to produce sluggish-lid or stagnant-lid modes in 3-D spherical geometry, Ratcliff et al. [1995, 1997] noted that sluggish-lid convection produces a more Venus-like distribution of surface features than stagnant-lid convection. From 2-D numerical models and scaling relationships, however, Solomatov and Moresi [1996] determined that stagnant lid convection is appropriate for Venus with a lithospheric thickness of 200–400 km on average. Such a large thickness does not allow Venus to lose its heat, so Solomatov and Moresi [1996] proposed that Venus had plate tectonics through most of its history, transitioning only recently to a stagnant lid. Convection scalings for stagnant lid convection with dislocation-creep rheology show that Venus can only lose 10–20 mW/m² before widespread mantle melting occurs [Reese et al., 1998]. With such a rheology and a relatively cold start, Reese et al. [1999] found that there could be a substantial time delay before the onset of melting.

[14] The possible cause of global resurfacing was investigated by several authors. A transition from layered to whole mantle convection caused by the endothermic spinel to perovskite phase transition was suggested by Steinbach and Yuen [1992] to have caused the global resurfacing event. Weinstein [1996] found that the interaction of phase-change induced avalanches with non-Newtonian lithospheric rheology can cause lithospheric overturn events. For the case that the lithosphere yields at a particular stress, Fowler and O'Brien [1996] presented mathematical analysis showing that episodic lithospheric overturn could result. Such episodic overturn events were subsequently obtained in numerical convection models with a strongly temperature-dependent, yielding rheology, in 2-D [Moresi and Solomatov, 1998] and in 3-D [Loddoch et al., 2006; Stein et al., 2010; Tackley, 2000; Trompert and Hansen, 1998]. Some recent modeling studies have found a coupling between surface mobility (either continuous or episodic) and climate-induced changes in surface temperature [Lenardic et al., 2008; Noack et al., 2012].

[15] Compositional variations caused by partial melting and crustal formation could play a major role, motivating models of coupled convection and magmatic differentiation. In a pioneering study, Dupeyrat and Sotin [1995] found that buoyant depleted mantle tends to accumulate below the lithosphere and suppress downwellings, while dense eclogite promotes recycling of the basaltic crust and limits crustal thickness to the depth of the basalt-eclogite transition, although they did not include temperature-dependent viscosity, which might stabilize the base of the crust. Ogawa

[2000] presented a more complex model including strongly temperature-dependent viscosity and the density crossover between basalt and harzburgite (or pyrolite) below the spinel to perovskite transition; that is, while basalt is relatively dense throughout most of the mantle, it is less dense for several tens of km at the top of the lower mantle because the transition to perovskite occurs at greater pressure in the basalt mineralogy [Ringwood, 1991]. Ogawa [2000] found substantial crustal recycling despite a high-viscosity lid, with the recycled crust building up above the core-mantle boundary (CMB) and at the base of the transition zone. The episodic breakdown of local chemical layering around 660 km depth caused by the composition-dependent phase transition resulted in massive “flushing events” causing vigorous magmatic pulses that might account for resurfacing events. Such intermittent chemical layering around 660 km caused by the basalt density inversion was also found in many other models studying Earth [e.g., Fleitout et al., 2000; Fujita and Ogawa, 2009; Nakagawa and Buffett, 2005; Nakagawa et al., 2009; Ogawa, 2007; Ogawa and Nakamura, 1998; Tackley et al., 2005; Xie and Tackley, 2004a, 2004b], and was revisited for Venus by Papuc and Davies [2012] although they point out that their model is not representative of Venus due to having neither a stagnant lid nor episodic lid overturn.

1.6. This Study

[16] We have performed numerical modeling of the thermochemical evolution of Venus over 4.5 billion years, using a model of coupled magmatism and convection in a spherical annulus [Hernlund and Tackley, 2008] or a 3-D spherical shell, with strongly temperature-dependent viscosity and either a stagnant lid, or episodic lid overturn induced by plastic yielding. Here we present the 2-D models and focus on how Venus loses its heat, and whether the results match (in a statistical sense) Venus's topography and geoid and its resurfacing history.

2. Model and Method

[17] The physical model and solution method are almost identical to those used in a series of Earth modeling papers [e.g., Nakagawa and Tackley, 2005a, 2010; Nakagawa et al., 2009, 2010] and similar to that in a recent Mars modeling paper [Keller and Tackley, 2009], with parameters suitably adjusted for Venus's slightly smaller size (compared to Earth) and with a more realistic viscosity variation with temperature. We here describe the key features and refer to previous publications for full details. The infinite Prandtl number approximation is assumed, and compressibility is included using the truncated anelastic approximation. Physical properties viscosity, density, thermal expansivity and thermal conductivity thus vary spatially as described below. The assumed values of physical properties are listed in Table 1.

2.1. Rheology

[18] The constitutive law is that of Newtonian (diffusion) creep plus, in some cases, plastic yielding. The parameters for diffusion creep are chosen to be “realistic,” i.e., based on laboratory values for the upper mantle [Karato and Wu, 1993], and best estimates for the lower mantle minerals [Yamazaki and Karato, 2001]. Specifically, we assume a

Table 1. Physical Properties^a

Property	Symbol	Value
Planetary radius	R	6052 km
CMB radius	R _{CMB}	3110 km
Mantle depth	D	2942 km
Gravity	g	8.87 m/s ²
Surface temperature	T _{surf}	740 K
Initial CMB temperature	T _{CMB_init}	4025 K
Specific heat capacity	C _p	1200 J/kg/K
Latent heat of melting	L	600 kJ/kg
Internal heating: present	H _{present}	5.2 × 10 ⁻¹² W/kg
Internal heating: initial	H _{init}	18.77 × 10 ⁻¹² W/kg
Half-life	t _{half}	2.43 Ga

^aSee figures and text for ones not listed.

temperature- and depth-dependent viscosity with different parameters for the upper and lower mantles:

$$\eta(T, d) = \eta_0 \exp \left[\frac{E + Bd}{RT} - \frac{E}{RT_0} \right] \quad (1)$$

where T is absolute temperature, d is depth, E is the activation energy, R is the gas constant, and B is related to the activation volume V by $B = \rho g V$, where g is the gravitational acceleration and ρ is a representative density for the region of interest. η_0 is the viscosity at temperature T₀ and zero pressure.

[19] For the upper mantle, the parameters are for dry olivine from *Karato and Wu* [1993], with an activation energy of 300 kJ/mol and an activation volume of 6 cm³/mol. For the lower mantle, E and B are chosen to give, based on *Yamazaki and Karato* [2001], a linear increase of activation enthalpy from 340 kJ/mol at the top of the lower mantle to 520 kJ/mol at the core-mantle boundary, which corresponds to an activation volume of about 2 cm³/mol. The absolute viscosity value is uncertain because the grain size is unknown; thus we vary the upper mantle reference viscosity, which is defined at the reference temperature T₀ = 1600 K, between 3 × 10¹⁹ and 2 × 10²⁰ Pa s, corresponding to grain sizes of 0.6 mm to 1.2 mm according to the equations and parameters in *Karato and Wu* [1993]. We have also tried values outside this range, but the results are less representative of Venus so are not

included here. There is a viscosity jump of factor 30 between the upper and lower mantles. The viscosity is truncated at 6 orders of magnitude higher, and 10 orders of magnitude lower, than the reference viscosity. The rheology is independent of composition in this initial study.

[20] The viscosity variation with depth along an adiabat with potential temperature 1600 K is plotted in Figure 1; also plotted is the viscosity profile along the same adiabat with or without idealized thermal boundary layers included at top and bottom (the so-called Venotherm). This shows that the viscosity in the deep mantle above the thermal boundary layer is about 10⁵ times higher than the reference viscosity, while the viscosity at the CMB is about 10 times higher than the reference viscosity, with a factor ~10⁴ viscosity decrease over the lower boundary layer. In the upper mantle, a minimum in viscosity occurs just below the lithosphere due to the activation volume; this indicates that an asthenosphere is expected to exist even with a dry rheology, contrary to some previous claims. Such a viscosity profile is consistent with constraints for Earth coming from mineral physics [e.g., *Steinberger and Calderwood*, 2006] and/or inversion of data coming from post-glacial rebound, geoid and seismology [e.g., *Mitrovica and Forte*, 2004], and rotation [*Peltier and Drummond*, 2010].

[21] In cases where plastic yielding is included, the yield stress is the minimum of that predicted by Byerlee's law with a friction coefficient of 0.5 and zero cohesion, and a constant yield stress to mimic semibrittle, semiductile processes in the lithosphere [*Kohlstedt et al.*, 1995]. Numerically, if the stress at given location exceeds the yield stress, the effective viscosity is reduced accordingly, and iterations must be done to obtain a consistent velocity-pressure solution and effective viscosity, as is normal practice in the community [e.g., *Moresi and Solomatov*, 1998; *van Heck and Tackley*, 2008]. We have run cases with various values of yield stress, and select a value of 100 MPa for the cases presented here because this leads to well-defined episodic overturn events corresponding to a popular hypothesis for Venus's evolution. Yield stress values that are significantly lower (less than about 50 MPa) lead to more continuous mobile-lid behavior whereas higher values lead to more local overturn events and

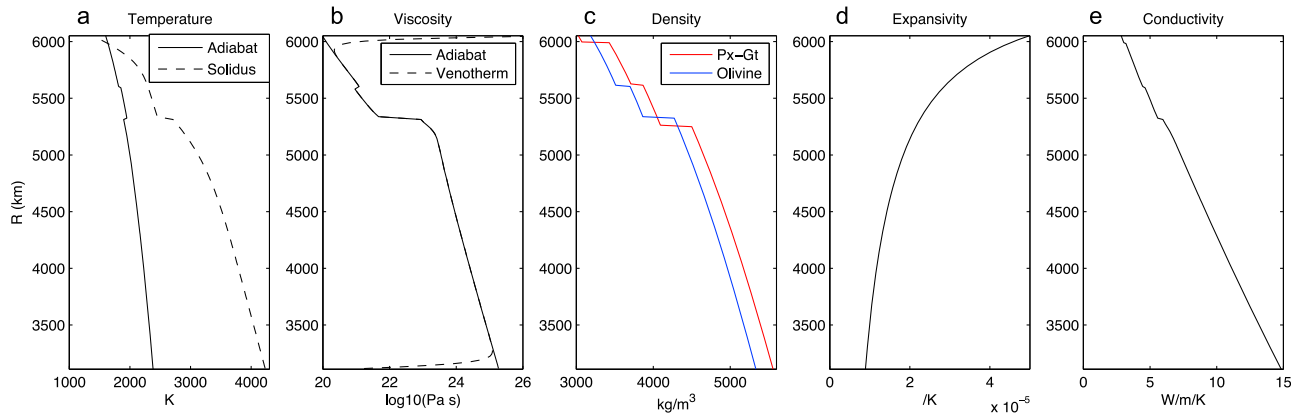


Figure 1. Radial profiles of various quantities as labeled from left to right: Temperature along an adiabat with 1600 K potential temperature together with the assumed solidus; viscosity along the 1600 K adiabat with $\eta_0 = 1 \times 10^{20}$ Pa s as well as a “Venotherm” consisting of the adiabat with idealized boundary layers at top and bottom; density for the olivine and pyroxene-garnet mineralogies; thermal expansivity; and thermal conductivity.

Table 2. Phase Change Parameters

Depth (km)	$\Delta\rho$ (kg/m ³)	γ (MPa/K)
<i>Olivine System</i>		
453	180	+2.5
730	400	-2.5
<i>Pyroxene-Garnet System</i>		
66	350	0
442	150	+1.0
796	400	+1.0

eventually a stagnant lid [e.g., *Moresi and Solomatov*, 1998]. Quantitatively, a yield stress of 200 MPa gives a series of overturn events although less vigorous and dying out after ~ 3 Ga, while a yield stress of 300 MPa gives overturn events for only ~ 1.5 Ga followed by a stagnant lid.

2.2. Composition, Melting, and Eruption

[22] Composition is assumed to vary between the two end-members basalt and harzburgite, with the fraction of basalt at each location given by the variable C , which varies from 0 to 1. Initially, the composition is homogeneous with $C = 0.2$ everywhere, consistent with the bulk composition of Earth's mantle [Xu et al., 2008]. Compositional variations are assumed to arise only from melt-induced differentiation, which is treated in the same manner as in previous studies [e.g., *Nakagawa and Tackley*, 2004, 2005a, 2005b, 2010; *Nakagawa et al.*, 2009, 2010; *Xie and Tackley*, 2004a, 2004b]. In this treatment, after each time step the temperature in each cell is compared to a depth-dependent solidus (Figure 1a), and if the temperature exceeds the solidus then enough melt is generated to bring the temperature back to the solidus, if sufficient basaltic end-member is present. Only the basalt component can melt, which approximates the rapid increase in solidus temperature when all the garnet and clinopyroxene has been removed by melting [e.g., *McKenzie and Bickle*, 1988]. To approximate the slight increase of solidus temperature with melt extraction when these minerals are still present, the solidus temperature linearly increases by up to 150 K as the basalt fraction drops from 20% to 0, although this has been found to have a minimal effect on the model evolution. Due to the rapid velocity of melt migration compared to convection, in this initial study we make the end-member assumption that all of the generated magma immediately erupts at the surface, provided it is above the depth at which magma is no longer less dense than the solid [Reese et al., 2007; Stolper et al., 1981], here taken to be a rather deep 600 km. If melt is generated below this depth, then it is advected with the solid until it either freezes or rises to above the neutral buoyancy depth. In reality, some magma may not rise all the way to the surface, instead forming igneous intrusions [e.g., *O'Neill et al.*, 2007], so this possibility will be considered in a future study.

2.3. Radiogenic Heating and Depth-Dependent Physical Properties

[23] The radiogenic heating rate per unit mass is assumed to decay exponentially with time, and in most cases is spatially uniform. In order to test the influence of trace element partitioning we include one stagnant lid case (with the intermediate reference viscosity of 10^{20} Pa s) in which heat-producing elements partition between melt and solid and are

thereby concentrated into the basaltic crust. This is implemented as in *Xie and Tackley* [2004a, 2004b], which was based on *Christensen and Hofmann* [1994]: each tracer carries trace elements, which are partitioned between melt and solid using the standard partitioning equation. Here, a generic heat-producing element (HPE) is included rather than separately tracking U, Th and K. We assume an extremely low partition coefficient $D = 0.0001$, which means that when partitioning occurs, essentially all of the HPE goes into the melt. The amount by which crustal HPE concentration is enhanced depends on the melt fraction: for example if a parcel of mantle melts by a total of 5% to produce crust, the HPE concentration in the resulting crust is 20 times higher than it was in the source material. The globally averaged HPE concentration is the same regardless of whether it is spatially constant or undergoes melt-solid partitioning and, based on the similarity of heat producing element concentration in Venusian basalts to those in terrestrial basalts [Janle et al., 1992; Nimmo and McKenzie, 1997; Turcotte, 1995], is assumed to have the "bulk silicate Earth" (BSE) value of 5.2×10^{12} W/kg (at the present day), and an average half-life of 2.43 Ga.

[24] The physical properties density, thermal expansivity and thermal conductivity are dependent on depth and are calculated as described in [Tackley, 1996, 1998]. Figure 1 shows the resulting depth profiles of these, and also an adiabat with a potential temperature of 1600 K, which has jumps due to phase change latent heat. The specific heat capacity is assumed to be constant.

2.4. Phase Transitions

[25] The model includes the most important solid-solid phase transitions, which depend on composition by parameterizing separately the transitions in the olivine system and in the pyroxene-garnet system based on mineral physics data [e.g., *Irifune and Ringwood*, 1993; *Ono et al.*, 2001], as discussed by *Xie and Tackley* [2004b]. All compositions are assumed to be a linear mixture of these two mineralogies; thus overall density and other physical properties are a weighted average of those for each mineralogy. Specifically, basalt is assumed to be pure pyroxene-garnet, while harzburgite is 75% olivine. The included phase transitions are listed in Table 2, and correspond to the transitions normally included in Earth models, scaled to greater depth by Venus's lower gravity; for example the transition to perovskite and magnesiowüstite in olivine occurs at 730 km depth. Figure 1c shows the resulting density profiles for these two mineralogies along a 1600 K adiabat. The greater depth of the transition to perovskite in the pyroxene-garnet system causes basalt to be buoyant in the depth range 730–800 km, which can have important dynamical effects [Ogawa, 2000]. The effects of phase transitions on density and latent heat are included using effective heat capacity and thermal expansivity [Christensen and Yuen, 1985; Nakagawa et al., 2009].

[26] In this manner, the variation of density with composition is taken into account, including the basalt-eclogite transition, the reduction in density as melt is removed (harzburgite is less dense than basalt), the basalt density inversion at the top of the lower mantle, and the relatively high density of basalt in the deep mantle [e.g., *Hirose et al.*, 2005; *Ohta et al.*, 2008].

[27] Two of the presented cases have phase transitions “switched off,” which means that Clapeyron slopes are set to zero and the depth of the garnet to perovskite transition is set to 730 km, the same as for the olivine system, thereby eliminating the basalt density inversion below 730 km.

2.5. Boundary and Initial Conditions

[28] The surface and core-mantle boundaries are isothermal and free slip, and the domain is periodic in the azimuthal direction. A surface temperature of 740 K is assumed. As in Earth, it seems likely that the core was substantially superheated directly after planetary formation and differentiation [Stevenson, 1990], therefore we set the initial CMB temperature to be higher than the mantle adiabat, at a conservative 4025 K (similar to Earth’s present-day CMB temperature). The model core cools as heat is removed by the mantle according to the parameterization given in [Nakagawa and Tackley, 2004] based on the earlier works by Buffett *et al.* [1992, 1996], which takes into account latent heat release, gravitational energy release caused by inner core growth, and radiogenic potassium with the concentration found to be necessary to give a successful evolution for Earth by Nakagawa and Tackley [2010]. The initial temperature field is adiabatic with a potential temperature of 1900 K, plus thin boundary layers at top and bottom and random (white noise) perturbations with a peak-to-peak amplitude of 25 K.

2.6. Solution Method

[29] We use the code StagYY [Tackley, 2008] in a spherical annulus geometry [Hernlund and Tackley, 2008]. StagYY uses a finite-volume, primitive variable discretization, solves the velocity-pressure solution using a multigrid solver, advects the temperature field using the MPDATA advection technique [Smolarkiewicz, 1984] and uses tracer particles to track composition and melt [Tackley and King, 2003]. Although we here report only 2-D spherical annulus results, StagYY is capable of modeling a fully 3-D spherical shell using the yin-yang grid; results in this geometry will be reported in a future paper. A full description of the method and benchmark tests are given in Hernlund and Tackley [2008] and Tackley [2008]. The grid resolution used is 512x64 cells, with 1 million tracers (about 30/cell). Test cases with a higher number of grid points and tracers show no significant difference in the features discussed here.

2.7. Geoid and Topography

[30] The self-gravitating geoid is calculated using a spectral method similar to that reported by Zhang and Christensen [1993] and Zhong *et al.* [2008], modified for compressibility. We here focus on the longest wavelengths so that elastic effects can be ignored [Steinberger *et al.*, 2010], although Golle *et al.* [2012] argue that it may be important even at these wavelengths. Admittance ratios are calculated using the usual assumption that the total gravity for each spherical harmonic is given by a correlated and uncorrelated component [Kiefer *et al.*, 1986; Simons *et al.*, 1994].

$$G_{lm} = F_l T_{lm} + I_{lm} \quad (2)$$

where G_{lm} and T_{lm} are spherical harmonic coefficients of the geoid and topography respectively, I_{lm} is the part of the geoid that is not correlated with topography, and F_l is the

admittance ratio for each degree. The admittance ratios can be simply determined by:

$$F_l = \text{Re} \left(\frac{\sigma_{gt}^2}{\sigma_{tt}^2} \right) \quad (3)$$

where σ_{gt} is the cross-covariance of geoid and topography, and σ_{tt} is the covariance of topography [Simons *et al.*, 1994].

2.8. Uncertainties

[31] In this initial paper, for space reasons we focus only on what are arguably the main uncertainties, which are the viscosity (dependent on unknown grain size and water concentration), whether or not the lithosphere can episodically overturn, and whether heat-producing elements partition into the crust. Various simplifying assumptions are made such as purely extrusive (as opposed to intrusive) magmatism, a crust that has the same rheology as the mantle, and no dislocation creep. It is worth considering uncertainties that may affect the results.

[32] After rheology (i.e., reference viscosity and yielding), the abundance of radiogenic heat-producing elements in Venus is perhaps the next most uncertain parameter due to only a few direct measurements having been made (see Turcotte [1995] for a summary). Physical properties such as thermal expansivity, thermal conductivity, density and their pressure-dependence are comparatively well known (see review in Tackley [2012]). Phase changes (pressures, Clapeyron slopes) and their compositional dependence still have some uncertainty although increasingly refined methods and databases for calculating phase equilibria over the mantle (temperature, pressure, composition) range are becoming available [Stixrude and Lithgow-Bertelloni, 2011; Nakagawa *et al.*, 2010].

[33] The greatest uncertainties probably come from modeling approximations rather than parameters. In particular, intrusive magmatism could cause quite different dynamics than extrusive magmatism, by heating and weakening the crust. This would strongly influence crustal tectonics, as would using a more realistic rheology for crustal materials and including dislocation creep. The melting/petrological model is highly simplified and the depth from which melt may ascent has much uncertainty that could strongly affect magmatism [Reese *et al.*, 2007]. If water were initially present and were progressively degassed this could have a notable effect on viscosity hence thermal evolution.

3. Stagnant Lid Results

3.1. Evolution of Thermochemical Structure

[34] The evolution of potential temperature (i.e., temperature extrapolated adiabatically to the surface; we plot this because plots of total temperature are dominated by the adiabatic gradient making it difficult to see convective features) and composition fields for the reference case is shown in Figure 2. The main features visible in the thermal field are several hot plumes, which move around with time. In the compositional field, the main feature is a layer of crust that forms very rapidly; by 500 Ma it is visible together with complementary depleted material in the upper \sim half of the mantle. Plumes from the CMB produce local regions of

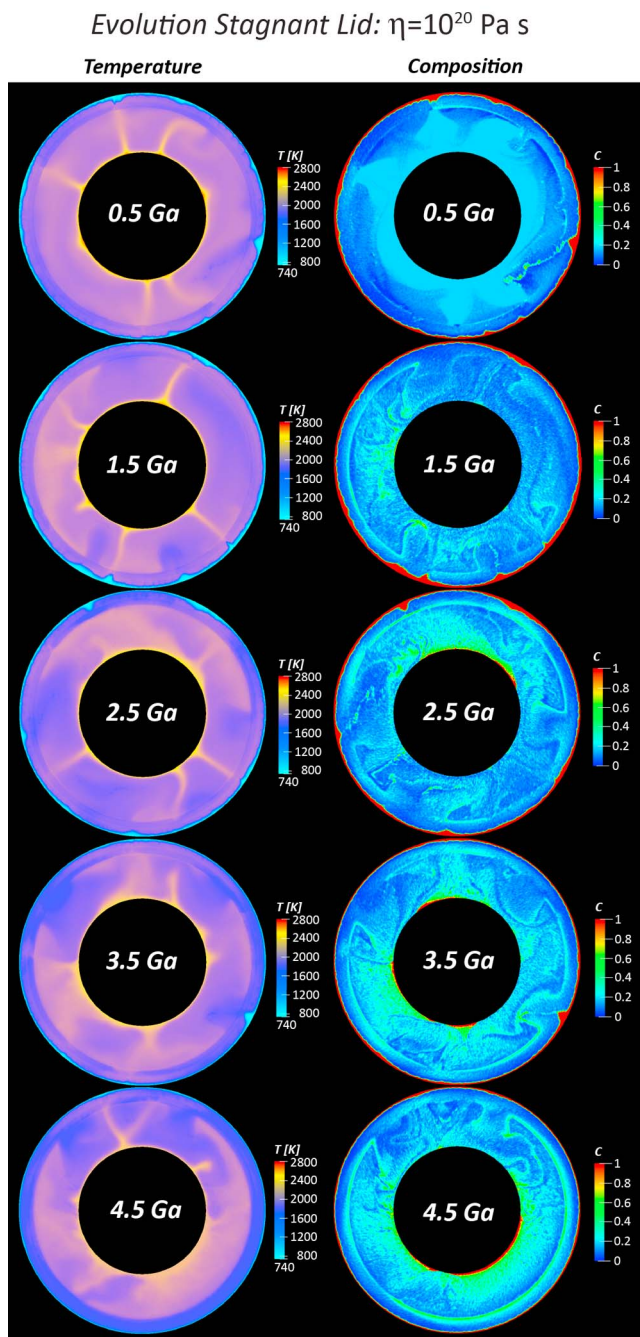


Figure 2. Time evolution of the potential temperature and composition fields for the stagnant lid case with reference viscosity 10^{20} Pa s, at half billion year intervals as labeled. The potential temperature scale ranges from 740 to 2800 K (note that a potential temperature of 2800 K corresponds to an actual temperature of about 4200 K at CMB pressure). Composition ranges from 0 (harzburgite) to 1 (basalt).

thicker crust. The plumes are quite time-dependent such that in one place a well-developed plume can be building a region of thickened crust while elsewhere plumes are either dying out or have not yet reached the lithosphere. Thus, even though plumes tend to have a characteristic size, at any particular time the associated surface volcanism will vary widely, qualitatively consistent with observations.

[35] The depleted material, despite being slightly buoyant (Figure 1 at 0.5 Ga), does not stay in the upper part of the mantle, but instead is mixed throughout the mantle by convection, such that by 1.5 Ga it is distributed throughout the mantle. Convection also entrains material from the base of the crust and mixes it throughout the mantle, with a small amount of settling of crustal material above the CMB.

[36] The crustal thickness is in a slowly evolving dynamic equilibrium, in which the production of new crust by melting and resurfacing is balanced by the removal of crust from its base by a mixture of entrainment by convective downwelling and remelting above upwellings. The equilibrium thickness of the crust decreases somewhat with time, such that by 4.5 Ga the crust is thinner than it was earlier in the evolution. From the thermal field it is evident that the crust is relatively cold, which is what is expected from rapid resurfacing and burial of old crust—the so-called “heat pipe” mechanism [Spohn, 1991; Stevenson and McNamara, 1988] discussed in Section 1.1.

[37] Local compositional layering is evident around 730 km depth, due to the different depths of the perovskite transition in basalt and harzburgite, as was previously found for Venus [Ogawa, 2000] and Earth (see Section 1.5) [e.g., Xie and Tackley, 2004a, 2004b]. Some episodicity in this local layering is apparent, with breakthrough of upper mantle material in “flushing events” or “avalanches” somewhat reminiscent of those identified in the early 1990s [e.g., Machetel and Weber, 1991; Peltier and Solheim, 1992; Tackley et al., 1993], although in the present results these are largely caused by compositional buoyancy rather than the negative Clapeyron slope.

3.2. Influence of Reference Viscosity

[38] The value of the reference viscosity (i.e., the viscosity at zero pressure and $T = 1600$ K) is the main uncertain parameter varied here. Figure 3 shows the final frames for cases with three different values of this, together with a case with phase transitions switched off. The main influence of reference viscosity seen in these figures is the crustal thickness: higher reference viscosity (giving a lower “effective” Rayleigh number) results in a thicker crust, while lower reference viscosity (giving a higher effective Rayleigh number) results in a thinner crust. This is because a higher viscosity results in lower convective heat transport at the same temperature, making the mantle heat up and therefore producing more and deeper melting, whereas lower reference viscosity facilitates more efficient heat transport, such that the mantle becomes less hot and melts less.

[39] Some secondary differences are also visible. A lower reference viscosity results in greater layering at 730 km (such that a temperature jump becomes visible in the temperature field) and slightly greater settling of delaminated basalt at the base of the mantle. The latter is consistent with the models of Davies [2006] although opposite to what was found by Christensen and Hofmann [1994], which may be due to greater temperature-dependence of viscosity in the present calculations and those of Davies [2006].

[40] The strong influence of composition-dependent phase transitions is indicated by the intermediate viscosity case with these switched off (i.e., same depth for both mineralogies; Clapeyron slopes = 0): there is no layering visible, but a greater propensity for depleted material to be in the

Present Day Stagnant Lid Cases

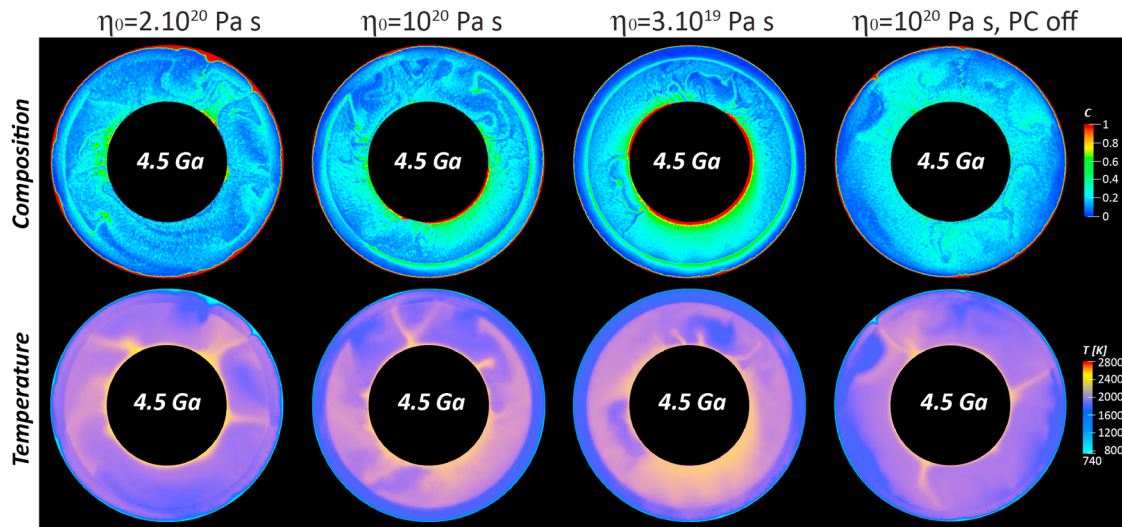


Figure 3. Final thermal and compositional structure for four stagnant lid cases: three with different reference viscosities as labeled, and one with the intermediate reference viscosity and phase transitions disabled. Scales as in Figure 2.

shallow mantle and for basaltic material to be in the deep mantle.

3.3. Thermal Evolution and Influence of Magmatism

[41] The thermal evolution, including the various contributions to the heat budget, is plotted in Figure 4 for three cases with different reference viscosity, plus a case with melting switched off and the intermediate reference viscosity.

[42] The heat budgets for the three cases with melting show that almost all of the total surface heat loss (red line) is magmatic (cyan line). Hence, almost all of the heat transport through the lithosphere in these models occurs by the magmatic heat pipe mechanism, which was discussed in Section 1.1. Heat conducted through the surface (blue line) is much lower, except toward the end in the cases with intermediate or low viscosity contrast, when it becomes comparable, due largely to a decrease in magmatic heat loss. In the low reference viscosity case, magmatic heat transport becomes less pronounced in the last ~ 1.5 Ga because convective heat transport is able to be more efficient. Total heat loss follows the same trend as radiogenic heat input but is larger due to heat from the core and (at some times) mantle cooling.

[43] Core heat loss (green lines) decreases monotonically with time, with superimposed small time-scale fluctuations. It is straightforward to explain the absence of a dynamo on Venus by the core heat loss being less than that conducted down the adiabat, although the latter quantity has a large uncertainty due to uncertainty in the thermal conductivity of the iron alloy at these conditions; a recent estimate places this higher than previously thought [Pozzo *et al.*, 2012]. The present-day value is around 9 TW for the higher reference viscosities and 4 TW for the lowest one. Early on, these models predict the core heat flow to be as high as 20–30 TW, thus there could have been a transition from geodynamo to no geodynamo. Even so, present-day model CMB heat fluxes for two of the models are in the range inferred for Earth of

5–15 TW [Lay *et al.*, 2008] so the difference in tectonic mode does not offer a straightforward explanation of the difference in dynamo presence between Earth and Venus.

[44] Plots of mean temperature versus time show that with melting included the temperature remains roughly constant throughout the planet’s history, at approximately 2400–2450 K, whereas when melting is switched off (cyan line) the temperature rises by almost 500 K to ~ 2870 K over the first ~ 3 billion years before decreasing. This is because melting plus magmatism is a very efficient heat loss mechanism and can strongly buffer the planetary temperature, as was predicted in parameterized models [Davies, 1990] and observed at early times in numerical models of Earth [Nakagawa and Tackley, 2012; Xie and Tackley, 2004a] and Mars [Keller and Tackley, 2009; Ogawa and Yanagisawa, 2011]. The heat budget for the no-melting case shows that surface heat loss is lower than radiogenic heat input for the first ~ 2.5 Ga, which is because stagnant lid convection is limited in its heat transport abilities.

[45] The temperature plot indicates only minor differences in temperatures for the three melting cases, i.e., of less than 100 K. In the first ~ 2.5 Ga, higher reference viscosity seems to result in higher temperature, consistent with the explanation offered above. This changes in the last ~ 1.5 Ga, with the low-viscosity case becoming hotter. Examination of the temperature distribution (Figure 3) shows that this is because of layering at 730 km: the lower mantle heats up because less of its heat is lost by advection across 730 km.

[46] The rms. velocity is also quite similar for the three melting cases, dropping from ~ 10 cm/yr near the beginning to ~ 2 cm/yr near the end. Some time-dependence is observed, particularly in the low-viscosity case. As shown later, this is accentuated by the effect of “avalanches” (episodic breakdown of layering) at the 730 km boundary. In the no-melting case, rms. velocity remains high throughout the history, because of the high temperatures hence low mantle viscosity.

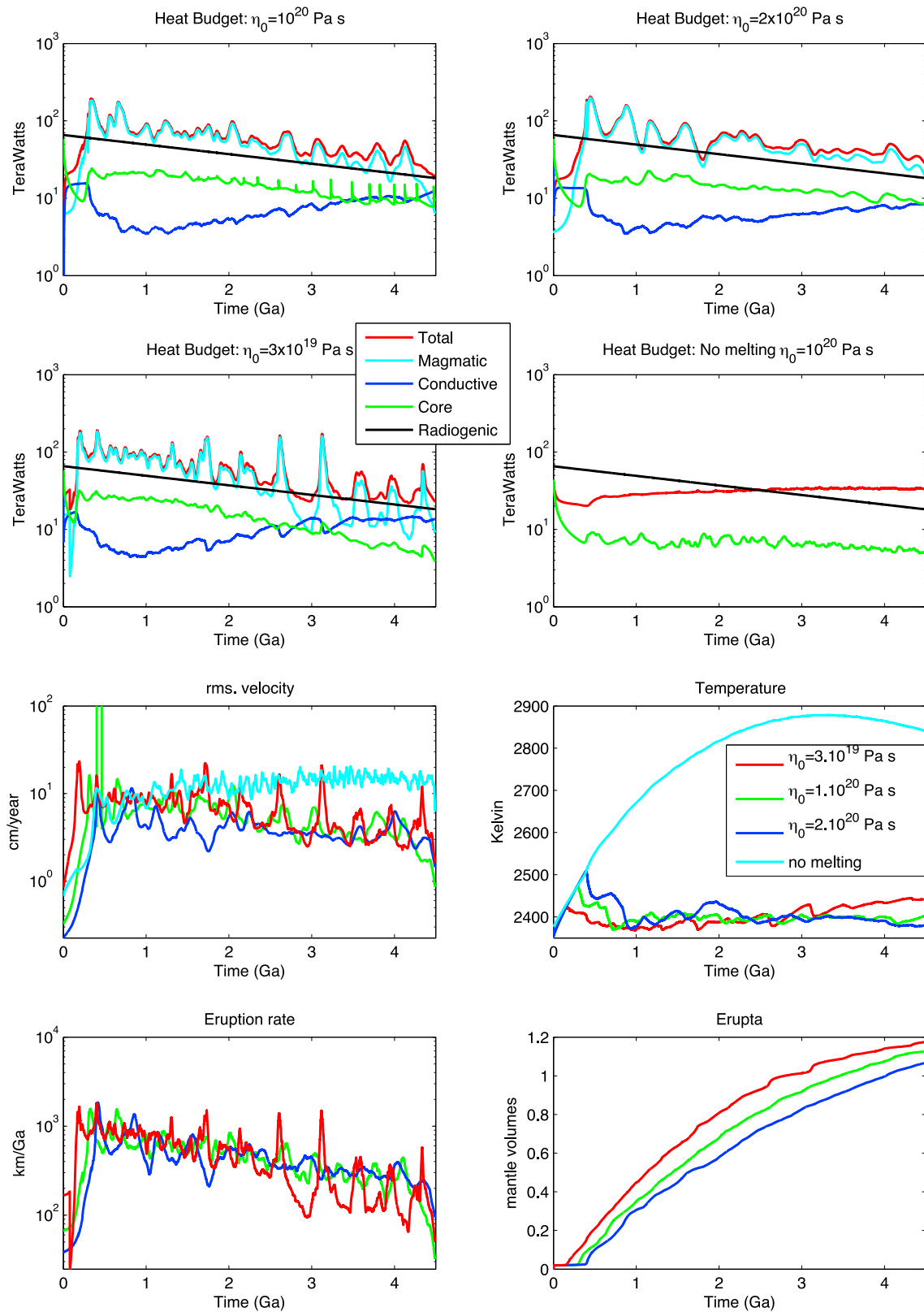


Figure 4. Time evolution of heat budget, rms. velocity, temperature, eruption rate and total erupted for the four stagnant lid cases shown in Figure 3. (top) The heat budget curves show total surface heat flow (red), surface heat flow due to magmatism (cyan), surface heat flow by thermal conduction (blue), heat flow across the core-mantle boundary (green), and radiogenic heating (black). (bottom) The lower four graphs contain curves for $\eta_0 = 3 \times 10^{19}$ Pa s (red), $\eta_0 = 1 \times 10^{20}$ Pa s (green), $\eta_0 = 2 \times 10^{20}$ Pa s (blue), and no melting (cyan), as shown in the legend.

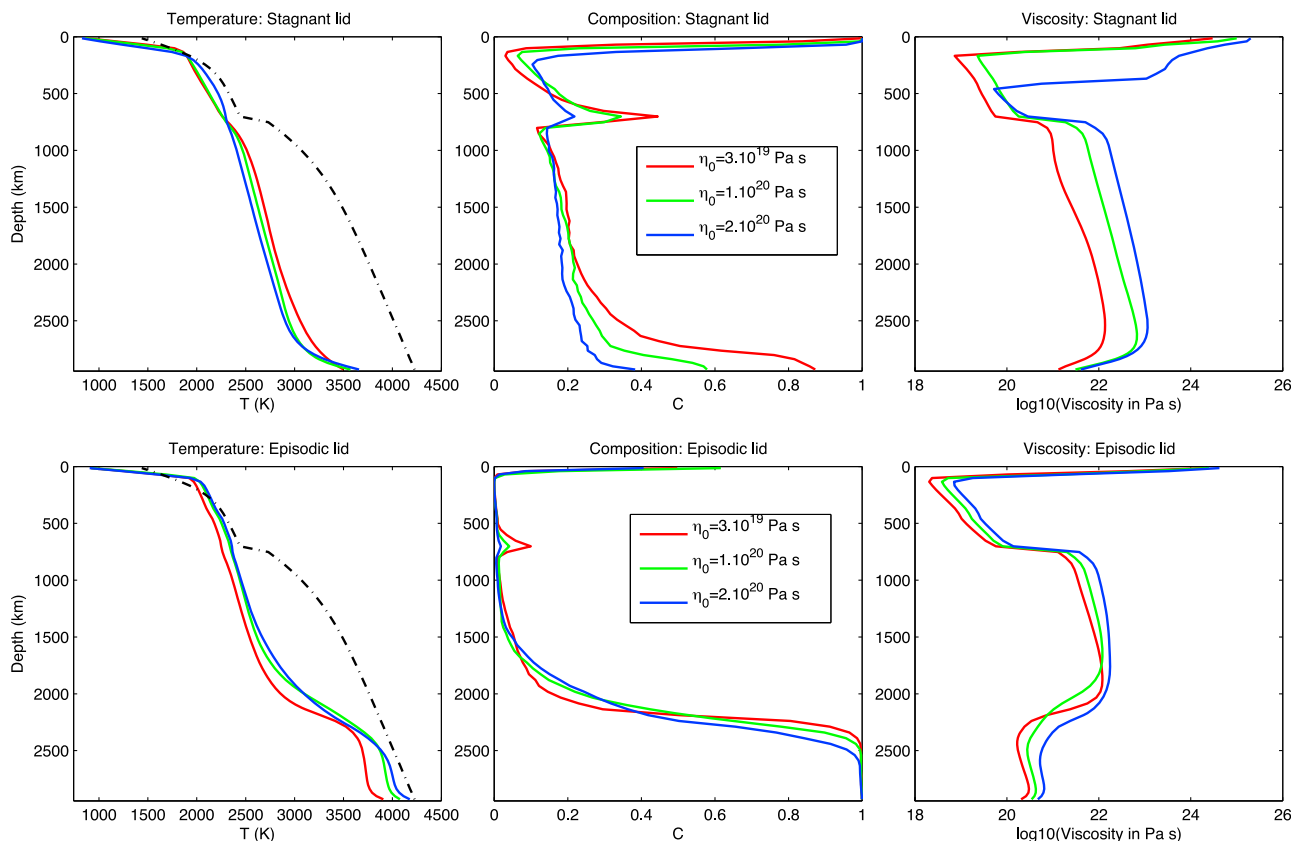


Figure 5. Radial profiles of horizontally averaged (left) temperature, (middle) composition, and (right) viscosity for the final state (after 4.5 Ga). (top) Stagnant lid cases and (bottom) episodic lid cases with the same reference viscosities. Line colors mean the same as in Figure 4, as also indicated in the legends.

[47] Eruption rate is also reasonably similar between the different cases, but with some fluctuations of up to an order of magnitude in the low-viscosity case, which is due largely to episodic breakdown of layering around 730 km depth. Eruption rates in the last 0.5 Ga are approximately 300 km of crust per Ga, consistent with the estimate in Section 1.1 of the resurfacing rate needed to lose Venus's internal heating and not consistent with the surface age estimates.

[48] The integrated eruption rate, i.e., total erupta, is slightly larger for the lower viscosity case. This may seem to contradict having thicker crust in the high-viscosity case, but this may be due to less efficient removal of the crust from its base (by convection) and a slower supply of fresh material to the base of the melting zone. The decrease in melting rate for the low-viscosity case toward the end is due partly to depletion of the shallow mantle due to compositional stratification. The integrated crust production, at over 1 mantle volume, indicates that crust is cycled multiple times over the planets' history.

[49] In the well-established theory of stagnant lid convection [e.g., Moresi and Solomatov, 1995], the equilibrium configuration is that convection takes place at a small temperature contrast (the rheological temperature contrast) below the stagnant lid such that the interior temperature is close to the CMB temperature. Such an equilibrium is never reached in these calculations because the core is hot and cools relatively slowly, while the mantle temperature is strongly

buffered by melting. Thus, plumes from above the CMB exist throughout the evolution.

3.4. Radial Structure

[50] Radial profiles of azimuthally averaged temperature, composition, and viscosity are plotted in Figure 5. The model Venotherms are hotter than a typical Earth geotherm (i.e., ~ 1600 K adiabat as plotted in Figure 1). Increasing reference viscosity leads to a thicker thermal lithosphere and higher upper mantle temperature (which 'touches' the solidus) but conversely, a lower temperature in the lower mantle. The latter is because of the decreasing effect of the composition-dependent phase transition in enforcing layering, which was also found for purely thermal convection [Christensen and Yuen, 1985; Yuen et al., 1994].

[51] The compositional profiles also show increasing compositional stratification around 730 km depth with decreasing reference viscosity, with basalt trapped at the base of the transition zone. Lower reference viscosity also results in greater accumulation of basalt above the CMB (as discussed above) and a thinner crust.

[52] In the viscosity profiles, it is evident that the upper mantle viscosity varies less between the cases than expected by the difference in their reference viscosities, because higher reference viscosity leads to a hotter upper mantle. Upper mantle viscosities are in the range 10^{19} – 10^{20} Pa s, depending on depth and case. The relatively high viscosity between 200 and 400 km depth in the high-reference viscosity case is due

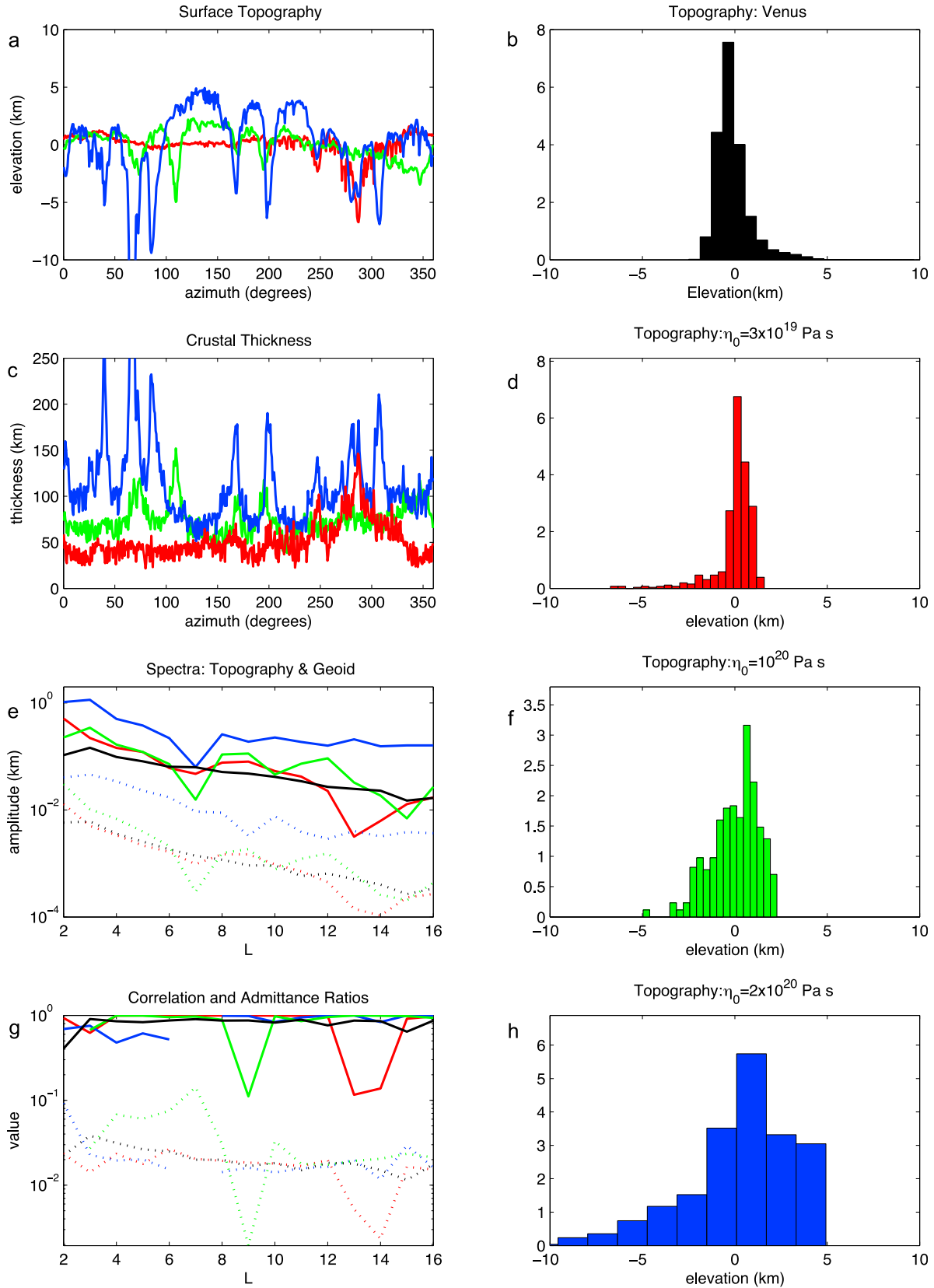


Figure 6

to locally thickened crust/lithosphere visible around the 1 o'clock position on Figure 3; because arithmetic averaging is used this strongly influences the global average (logarithmic, i.e., geometric averaging would give a profile that more reflects the temperature field). Lower mantle viscosities are in the range 10^{21} – 10^{23} Pa s and vary more than expected between the different cases, because lower reference viscosity leads to a higher lower mantle temperature, amplifying the lower viscosity.

3.5. Topography, Crustal Thickness, and Geoid

[53] The range of topographic variation, the amplitude and spectrum of the geoid, and the admittance ratios are some of the major constraints on Venus. These are analyzed and compared to Venus in Figure 6.

[54] The probability distribution (histogram) of Venus's topography (Figure 6b) is unimodal with a slight skew to high values. The distribution of topography in the numerical models (Figures 6d, 6f, and 6h) is also unimodal but if anything has a slight skew to lower values. Most diagnostic is the width of the distribution, i.e., the range in topography. In the models, the variation in surface topography increases with increasing reference viscosity, and seems to match Venus best for somewhere between 3×10^{19} and 10^{20} Pa s.

[55] The spatial variation in surface topography for the three cases is shown in Figure 6a, together with the corresponding crustal thickness (Figure 6c). The surface topography varies smoothly, with several valleys. Comparison with the crustal thickness (Figure 6c) indicates an anticorrelation: low-lying regions have thicker crust and high regions have thinner crust. This is opposite to what is normally expected for a buoyant crust in isostatic equilibrium, and occurs because the base of the crust is in the eclogite stability field, i.e., it is denser than the underlying mantle. Regions of thicker crust therefore contain a larger amount of dense eclogite and sink lower. We have verified this interpretation by moving the eclogite transition much deeper and recalculating topography: in that case the conventional positive topography/thickness correlation is observed.

[56] Gravity and its relationship to topography is another major constraint, so we here plot the spectra of geoid, surface topography and the admittance ratio, for the three cases (Figures 6e and 6g). We restrict our comparison to the longest wavelengths where elastic support of the lithosphere is generally thought to be unimportant [e.g., Steinberger *et al.*, 2010]. The spectrum of topography has approximately the right slope for Venus, and this plot again indicates that a reference viscosity in the range 3×10^{19} and 10^{20} Pa s gives the right amplitude. The same is true of the geoid. Correlation and admittance ratios are plotted in Figure 6g. These fields are well correlated at most wavelengths, with some exceptions. Admittance ratios fluctuate quite a lot from degree to degree, but are in the right ballpark for Venus for all three cases.

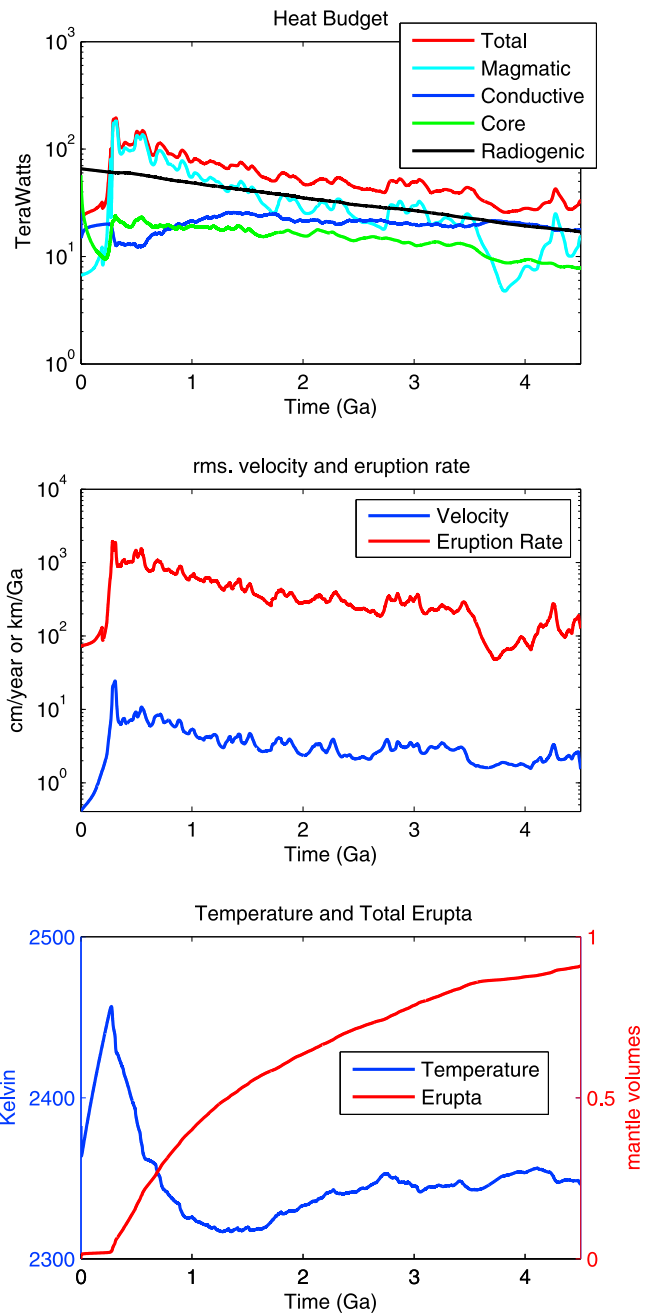


Figure 7. Time evolution of (top) heat budget, (middle) rms. velocity and eruption rate, and (bottom) total erupta and temperature, for the stagnant lid case with reference viscosity $\eta_0 = 1 \times 10^{20}$ Pa s and partitioning of heat-producing elements into the melt/crust. Color coding of heat budget lines is as in Figure 4. Velocity and temperature are blue, whereas eruption rate and total erupta are read, as per legends.

Figure 6. Topography and geoid diagnostics for three stagnant lid cases, with color coding as in Figures 3 and 4. (left) (top) The spatial variation of surface topography and crustal thickness; (bottom) spherical harmonic spectra of topography (solid lines) and geoid (dotted lines) compared to Venus (black lines); and geoid/topography correlation (solid lines) and admittance ratios (dotted lines) compared to Venus (black lines). Gaps correspond to negative values, which don't plot in log space. (right) Histograms of surface topography for Venus and the stagnant lid cases with $\eta_0 = 3 \times 10^{19}$ Pa s (red), $\eta_0 = 1 \times 10^{20}$ Pa s (green), $\eta_0 = 2 \times 10^{20}$ Pa s (blue). The Venus topography data are from Rappaport *et al.* [1999] and the geoid data from Konopliv *et al.* [1999].

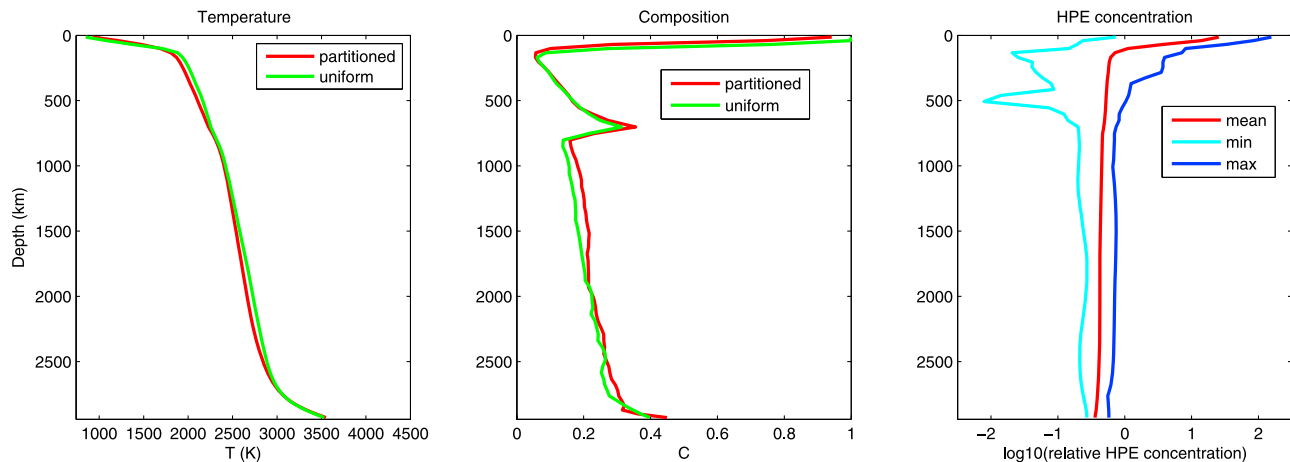


Figure 8. Radial profiles of temperature, composition (basalt fraction) and heat-producing element concentration for the stagnant lid case with partitioning of heat-producing elements into the melt/crust. (left and middle) The similar case with no partitioning is plotted for comparison.

[57] In summary, cases with a reference viscosity in the range 3×10^{19} and 10^{20} Pa s give a Venus-like range of topography, geoid and admittance ratios compared to Venus, whereas a higher reference viscosity results in too high variations in surface topography and geoid, although reasonable admittance ratios. While these cases might thus be thought to match Venus, a major problem is the huge rate of magmatic resurfacing that is necessary to lose the internal heating—about 2 orders of magnitude larger than the magmatic rate inferred for recent Venus (see review in Section 1.1). This motivates the exploration of models with episodic lid behavior (Section 4).

3.6. Influence of Heat-Producing Element Partitioning

[58] The time evolution of heat budget, rms. velocity, temperature, eruption rate and total erupta are shown in Figure 7, and may be compared with the intermediate reference viscosity (10^{20} Pa s) case in Figure 4. While the overall evolution appears similar, magmatic heat flux is somewhat lower: after a transient phase lasting just over 1 Ga the magmatic heat flux is similar to or lower than radiogenic heating, whereas with no HPE partitioning (Figure 4) it is similar to the total heat loss for most of the planet's history. Between ~ 3.6 and 4.2 Ga the magmatic heat flux is unusually low; this corresponds to a period when the flow is layered by the action of composition-dependent phase transitions near 730 km depth. Nevertheless, the present-day eruption rate (Figure 7, middle) is still high, at around 100 km/Ga. Due to the somewhat lower eruption rate, the total erupta corresponds to 0.9 mantle volumes compared to 1.1 mantle volumes for the case with no HPE partitioning. The mean temperature (Figure 7, bottom) is about 50 K lower than in the non-HPE-partitioning cases (Figure 4).

[59] Radial profiles of various quantities are plotted in Figure 8. Profiles of temperature and composition are very similar to the equivalent non-HPE-partitioning case but subtle differences are apparent: the crust/lithosphere is slightly warmer while the mantle is slightly colder (Figure 8, left) and the crust is slightly thinner (Figure 8, middle). Most interesting are the profiles of azimuthally averaged HPE concentration ($\langle \text{HPE} \rangle$), which are plotted relative to the average, i.e.,

corresponding to bulk silicate Venus (BSV), which is here assumed to be equal to bulk silicate Earth (BSE). In the mantle the average heating rate from HPE, $\langle H_{\text{HPE}} \rangle$ is in the range 0.4–0.5 H_{BSV} , while in the crust it rises to an azimuthal average of 26 H_{BSV} , with a maximum of 156 H_{BSV} . Large lateral variations occur in the upper mantle (where some depleted material with very low HPE exists) and in the crust. The crustal range of ~ 1 –150 H_{BSV} (average 26) encompasses the concentrations measured in Venus's crust, which range from 14 to 102 (see *Turcotte* [1995] and Section 1.1). Temperature and compositional fields resemble those of the case without HPE partitioning so are not plotted here.

[60] Thus, despite the very low partition coefficient assumed (0.0001), the system cannot reach a state in which HPE is entirely contained in the crust; instead about 45% of it remains in the mantle with a commensurate reduction in magmatic heat pipe transport. This is because while new highly radiogenic crust is being produced by melting, old highly radiogenic crust is being entrained into the mantle from the base of the crust, such that the HPE budget eventually reaches a dynamic equilibrium. Perhaps the only way to concentrate all HPE into the crust is as an initial condition resulting from, for example, magma ocean solidification, and this should be considered in future studies.

4. Episodic Lid Results

4.1. Evolution of Thermochemical Structure

[61] The evolution of thermal (potential temperature) and compositional fields for the case with the lowest reference viscosity is shown in Figure 9. These are markedly different from those for the stagnant lid cases, due to the effect of global lithospheric overturn events. At the times shown in the left panel at 0.5 Ga intervals, no overturn events are taking place; they occur relatively quickly between these frames. Thus, on the right is shown a detailed time sequence of a global overturn event that starts about 1.9 Ga into the simulation and lasts for about 150 Ma. It starts in one place then propagates around the planet until all of the lithosphere has sunk to the deep mantle. The crust is carried into the deep mantle and much of it settles into a layer above the

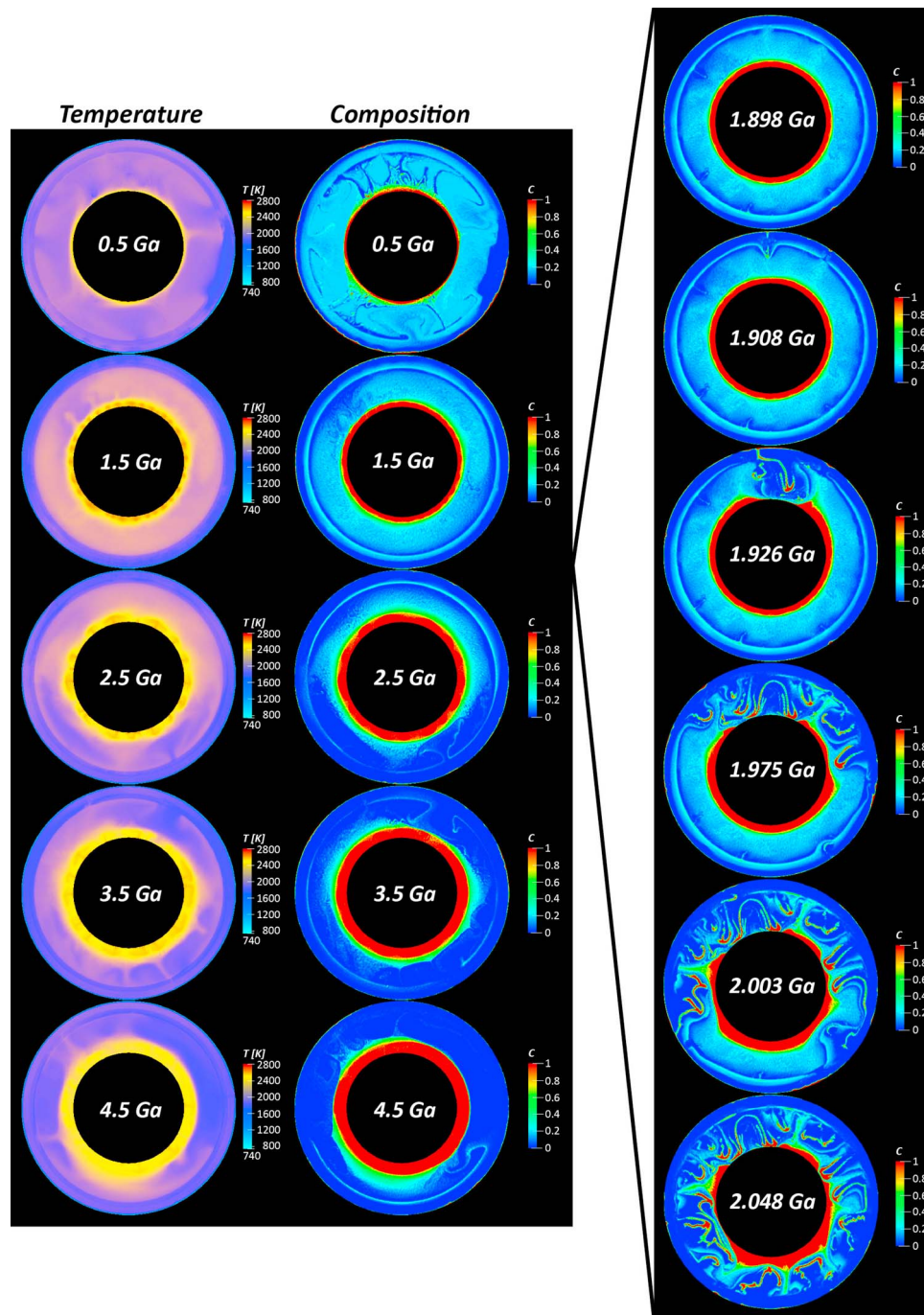


Figure 9. (left) Time evolution of the potential temperature and composition fields for the episodic lid case with reference viscosity 3×10^{19} Pa s, at half billion year intervals as labeled, plus (right) zoom-in of a global overturn event. As in Figures 1 and 2 the potential temperature scale ranges from 740 to 2800 K (note that a potential temperature of 2800 K corresponds to an actual temperature of about 4200 K at CMB pressure). Composition ranges from 0 (harzburgite) to 1 (basalt).

CMB, which develops internal convection. Thus, the net effect of multiple global overturn events is to strongly differentiate the mantle into a basalt-enriched layer at the bottom and a depleted harzburgitic layer above. The crust is quite thin compared to the stagnant lid cases.

[62] The value of the reference viscosity makes little difference to the visual appearance of these cases (Figure 10). All cases display a thin crust, a somewhat thicker lithosphere

and a layer of overturned crust in the deep mantle. Phase transitions also make little visual difference (right column).

4.2. Heat Budget

[63] Time series of the heat budget (Figure 11) are dramatically different from those of the stagnant lid cases. The periodicity is comparable to the estimated elapsed time since the last resurfacing on Venus. Heat is lost mainly in a series

Present Day Episodic Lid Cases ($\eta_0=100$ MPa)

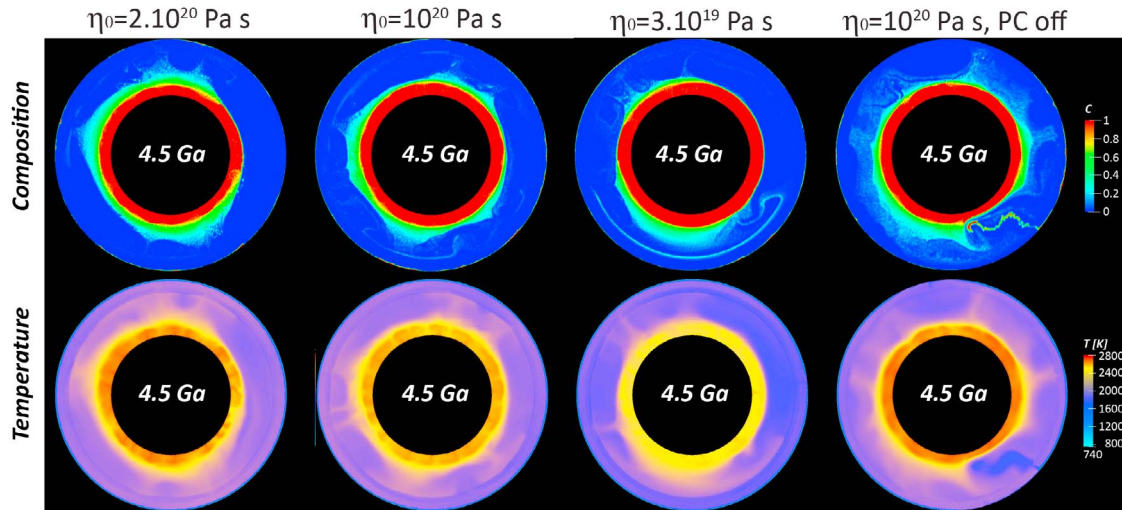


Figure 10. Final thermal and compositional structure for four episodic lid cases: three with different reference viscosities as labeled, and one with the intermediate reference viscosity and phase transitions disabled. Scale as in Figures 2, 3, and 7.

of pulses of high heat flux corresponding to global overturn events: about eight in the intermediate viscosity case, while between these the heat flux is lower than radiogenic heat input. Magmatic heat flow is only a small fraction of the total heat flow (again in contrast to the stagnant lid cases), except during the pulses. A lower reference viscosity (Figure 11c) results in more vigorous and fewer pulses (around 5), but otherwise the same character. A higher reference viscosity (Figure 11b) results in less vigorous pulses that last longer: a higher fraction of the time is spent overturning the lithosphere. The overturn events are clearly visible as spikes in the rms. velocity.

[64] Core heat flow (green lines) is quite high despite the core being surrounded by a layer of dense material, but is significantly lower than that in the stagnant lid cases, dropping to a present-day value of around 3 TW (early on it can be as large as 30 TW). Such a low value is probably too low for a dynamo to exist.

[65] Temperature displays a ‘ramped’ evolution, increasing during quiescent periods then dropping by up to 150 K during an overturn event. The final mean temperature is 100–200 K higher than in the stagnant lid cases, probably because of the high temperatures in the deepest mantle where basalt accumulates. Velocity and eruption rate also display a series of pulses and total erupta a stepped evolution, with the total amount of melting being about half that in the stagnant lid cases, consistent with a much smaller fraction of the heat flow being magmatic.

[66] Eruption (resurfacing) rates in the last 0.5 Ga are in the range 10–100 km/Ga, which is substantially (about an order of magnitude) lower than the 300 km/Ga found in the stagnant lid cases, although still high compared to observational constraints discussed in Section 1.1.

4.3. Radial Structure

[67] Radial profiles of azimuthally averaged temperature, composition and viscosity are plotted in Figure 5 (bottom).

Again, higher reference viscosity results in higher temperature (Figure 5, bottom left), which in turn reduces the contrast in viscosity between the different cases (Figure 5, bottom right). The temperature below the lithosphere now exceeds the pyrolite solidus, which is possible because the upper mantle is strongly depleted in the basaltic component and the solidus is increased by depletion.

[68] The profiles of composition show the layer of crust above the CMB, a thin crust, and a small amount of basalt accumulation above 730 km depth. Near the base of the mantle there are very high temperatures and quite low viscosities because of the dense layer of crust.

[69] The lithosphere is quite thin in these cases—about 100 km—even though the analyzed time is in a quiescent period. Conductive thickening of the lithosphere to 100 s km as proposed by *Turcotte* [1993] for episodic Venus evolution does not seem to occur in these simulations. During quiescent periods there is still convection taking place below the lithosphere, keeping it thin. The lithospheric thickness is roughly independent of reference viscosity, unlike in the stagnant lid cases. This reason for this difference may be the strong depletion of the upper mantle in the episodic lid cases, allowing the usual self-regulation of temperature and viscosity to occur in order to maintain \sim constant heat flux, whereas in the stagnant lid cases the lithospheric thickness is controlled by the intersection of the Venotherm with the solidus: higher reference viscosity leads to a hotter Venotherm hence thicker crust/lithosphere.

4.4. Topography, Crustal Thickness, and Geoid

[70] Figure 12 shows diagnostics related to topography, crustal thickness and geoid for the three episodic lid cases. The crustal thickness is typically in the range 10–50 km—much thinner than in the stagnant lid cases (Figure 6) and much more consistent with observational constraints (Section 1.1). A positive correlation between crustal thickness and topography is visible, as expected because the crust is not thick enough to

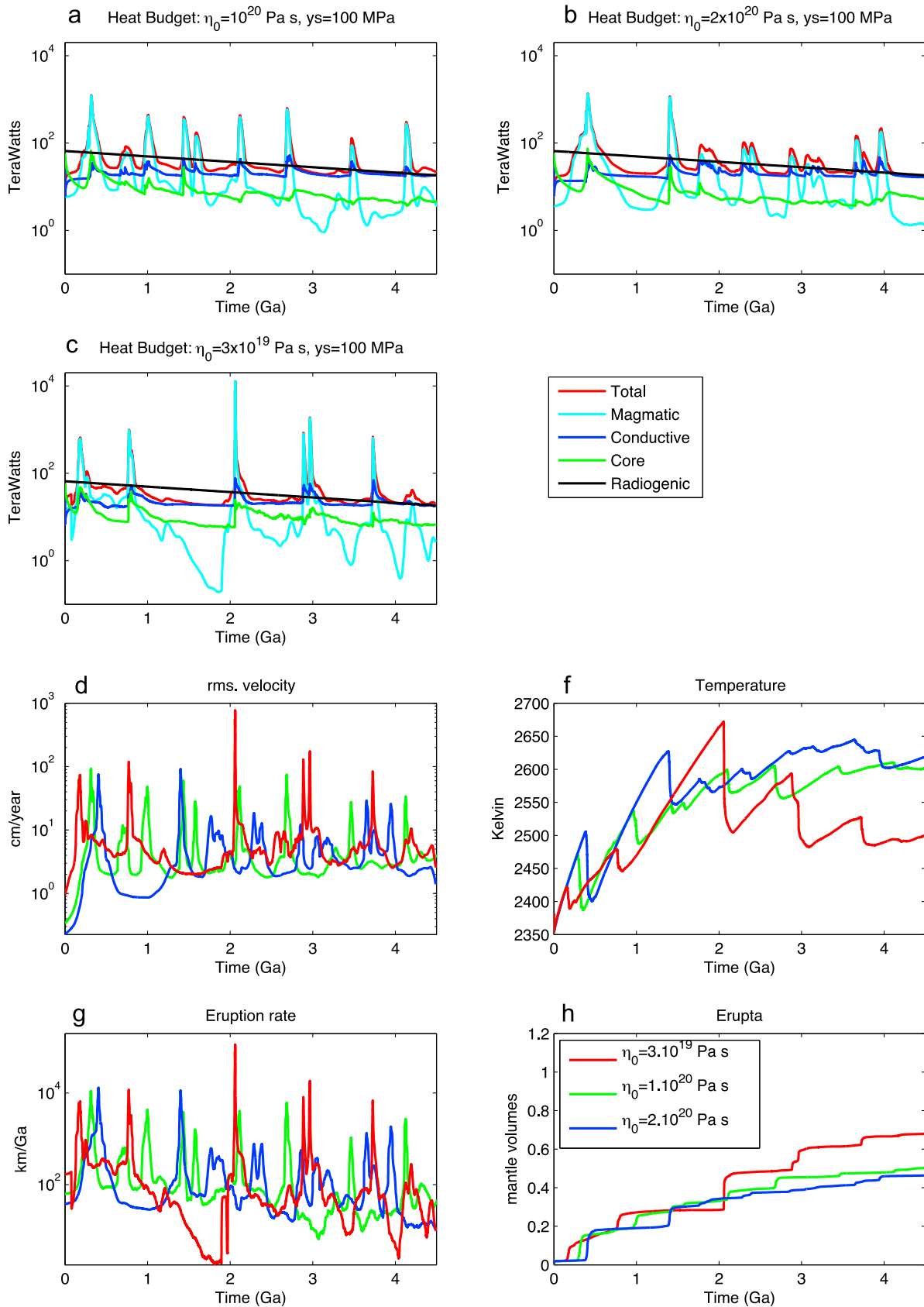


Figure 11. Time evolution of heat budget, rms. velocity, temperature, eruption rate and total erupta for the three episodic lid cases with phase changes included shown in Figure 8. The various curves are as in Figure 4 and the legends.

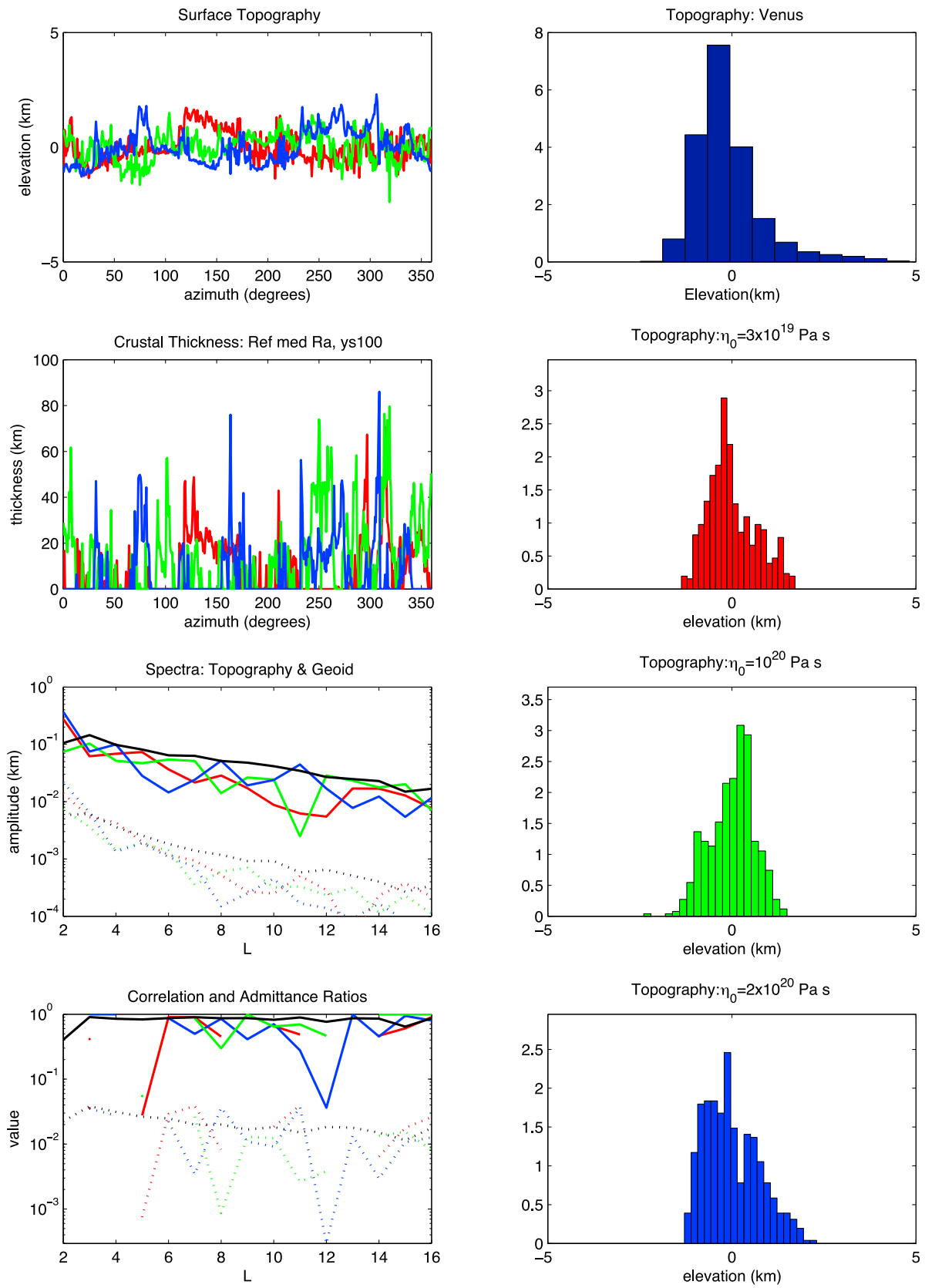


Figure 12. Topography and geoid diagnostics for three episodic lid cases, with color coding as in Figures 3, 4, 5, 6, and 9 and the same meanings as in Figure 6.

enter the eclogite stability field, in contrast to the stagnant lid cases.

[71] Histograms of topography for the three values of reference viscosity display roughly the same range, again in contrast to the stagnant lid cases where topography increased with reference viscosity. This could be because topography tends to scale with lithospheric thickness, which is smaller and less variable (with respect to reference viscosity) in the episodic lid cases. The range of topography is similar to that of Venus except without the skew toward high values.

[72] Spectra of topography and geoid are similar for all cases, and similar in amplitude to Venus at low harmonics (up to $L = 4$) but lower in amplitude above about $L = 5$. Geoid and topography are fairly well correlated, as observed on Venus. Admittance ratios are quite noisy from one degree to another, and are generally similar or lower than Venus's.

[73] In summary, both the topography and the spectra of geoid and topography appear to be quite noisy for these cases. The range of topography is similar to Venus's but in spectral space both topography and geoid are lower than Venus's except at the longest degrees.

5. Influence of Phase Transitions

[74] In all of the discussed cases the phase transition to perovskite, and the dependence of its depth on composition (i.e., it occurs deeper in basalt), causes local compositional stratification around 730 km depth, with basaltic material accumulating at the base of the transition zone and harzburgitic material accumulating at the top of the lower mantle, as has been discussed in several previous works discussed in Section 1.4 [e.g., *Ogawa*, 2000; *Tackley et al.*, 2005]. For Venus, it was suggested by *Papuc and Davies* [2012] that episodic breakdown of this local layering could be responsible for episodic volcanism on Venus, but they noted that their models are not representative of Venus because they have a continuously mobile lid, rather than being in stagnant lid or episodic lid modes. Thus, we here test this, by computing additional cases in which the phase transition to perovskite is "switched off," meaning that it is put at the same depth for both mineralogies, and the Clapeyron slope is set to zero.

[75] Temperature and compositional fields for stagnant lid and episodic lid cases with phase transitions switched off are shown in Figures 3 and 10, respectively. In the stagnant lid case this certainly makes a difference, with compositional heterogeneity more uniformly spread throughout the mantle. Additionally, the deep mantle is less hot due to the absence of layering at 660 and the absence of any crustal segregation above the CMB. For the episodic lid case a difference is less apparent, because most of the mantle is strongly depleted so there is not much basalt around 660 to be entrapped.

[76] Time series for both stagnant and episodic lid cases, comparing with and without phase changes, are shown in Figure 13. Heat budgets can be compared to equivalent cases with phase changes on (Figures 4 and 11). For the stagnant lid case (left column) the heat budget, rms. velocity and eruption rate display notably more time-dependence when phase changes are switched on, although the difference is smaller than the intrinsic time-dependence. The difference is also less than that between stagnant and episodic lid cases. A time series comparison for episodic lid convection is shown in Figure 13 (right). The pulses are somewhat higher and

shorter in the case with phase changes on, which is probably because lithospheric overturn occurs simultaneously with breakdown of the layering around 730 km, which amplifies the instability. Again, however, the influence of phase changes is smaller than the episodicity caused by the basic system dynamics. In both cases the eruption rate is slightly lower with phase changes on.

[77] In summary, episodic breakdown of layering around 730 km causes a noticeable increase in episodicity in these cases. In future this could be investigated for a wider range of plausible parameters; for example the low-reference viscosity stagnant-lid case display considerably more episodicity (Figure 4), which might be due to these phase changes.

6. Discussion and Conclusions

[78] Here we present numerical convection models to investigate the thermochemical evolution of Venus including heat loss mechanisms, and constrain the models by comparing to present-day topography and geoid and recent resurfacing history of Venus. The models include melting and magmatism, decaying heat-producing elements and core cooling, realistic temperature-dependence of viscosity leading to stagnant lid convection, and in some cases, plastic yielding to give episodic lithospheric overturn. One case includes strong partitioning of heat-producing elements into the melt/crust. The main parameter varied is the reference viscosity (i.e., the viscosity at 1600 K and zero pressure).

[79] The main conclusions are as follows:

[80] 1. If Venus was always in stagnant lid mode, our calculations predict that the dominant mode of heat transport across the lithosphere is magmatic heat pipe [*O'Reilly and Davies*, 1981; *Spohn*, 1991], which requires $\sim 170 \text{ km}^3/\text{yr}$ of crustal production at the present day, consistent with *Solomon and Head* [1982]. Such rapid resurfacing ($\sim 300 \text{ km/Ga}$) appears to be inconsistent with observations. Strong partitioning of heat-producing elements into the crust can reduce this to $\sim 100 \text{ km/Ga}$ —not enough to resolve the discrepancy. However, in some simulations the volcanic rate does decrease toward the end, so further investigation is needed to isolate the parameter range in which this occurs, bearing in mind the scenarios for cessation of volcanism identified in the parameterized models of *Reese et al.* [2007] and *Kite et al.* [2009].

[81] 2. Vigorous episodic lid overturn interspersed by periods of relative quiescence, as obtained in models with a yield stress of 100 MPa, is an effective method of losing Venus's heat while obtaining low rates of volcanism between bursts, and therefore offers the most straightforward way to match to observations of Venus. Our calculations predict 5–8 overturn events over the history of Venus. The length of each overturn event increases with the value of reference viscosity; 150 million years is typical. Overturn events initiate in one place (often where crust is thickened by volcanism) and propagate around the planet. However, this mode of convection is slightly different from that proposed by *Turcotte* [1993] in that the lithosphere does not thicken to 100s km during quiescent periods—instead convection keeps it thin, as discussed in Section 4.3.

[82] 3. The crustal thickness is large—from 40 km up to 150 km or more—in stagnant lid mode, and roughly equal to the rheological lithosphere as predicted by *Spohn* [1991]. In episodic mode, smaller crustal thicknesses averaging around

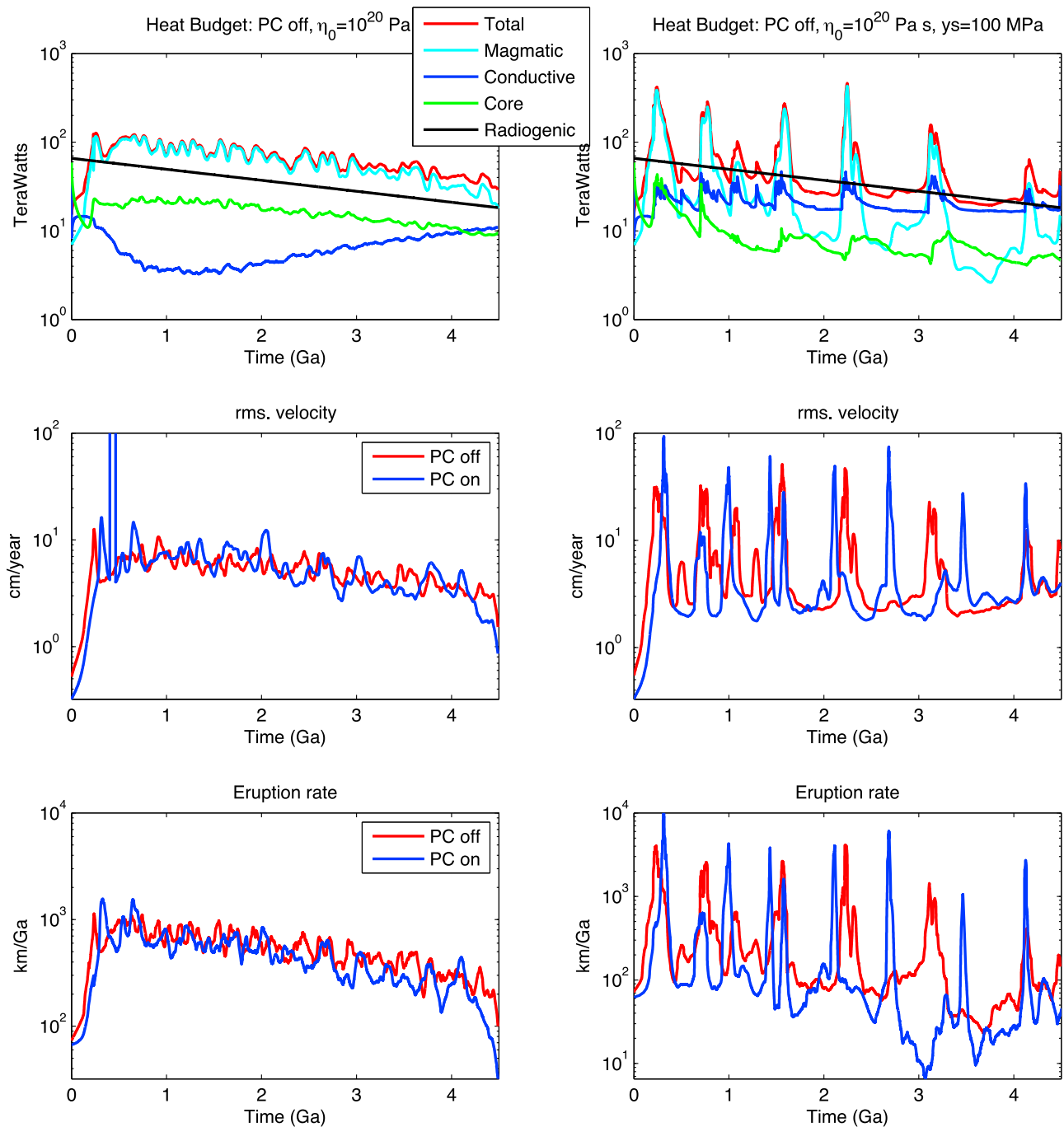


Figure 13. Time evolution of heat budget, rms. velocity, and eruption rate for the two cases with phase changes disabled and a reference viscosity of $\eta_0 = 1 \times 10^{20}$ Pa s as shown in the right columns of Figure 3 (stagnant lid) and Figure 10 (episodic lid). The color coding of heat budget plots is as in Figures 4 and 11 and the legend, while the velocity and eruption rate plots compare phase changes enabled (blue lines, as also plotted in Figures 4 and 9) and disabled (red lines).

30 km are obtained, which is more consistent with estimates of crustal thickness for Venus of 10–60 km (see Section 1.3 and review by *Breuer and Moore* [2007]; also *Anderson and Smrekar* [2006] find 0–90 km).

[83] 4. Crustal thickness is not limited by the basalt to eclogite transition (unlike in the models of *Dupeyrat and Sotin* [1995]) because the high viscosity at the base of the crust prevents rapid delamination. When the base of the crust

is composed of eclogite, regions of thicker crust are topographically low rather than high as they are with a smaller mean crustal thickness. A strong influence of the basalt-eclogite transition on topography was previously found by *Jull and Arkani-Hamed* [1995].

[84] 5. Crust is recycled in both tectonic modes: by entrainment from its base in stagnant lid convection, and by lid overturn in episodic lid mode. In episodic lid mode a

thick layer of subducted crust builds up above the CMB, whereas in stagnant lid mode entrained crust mostly mixes back into the mantle, with only a small amount segregating above the CMB.

[85] 6. Venus-like amplitudes of surface topography and geoid can be produced in either stagnant lid or episodic lid modes, although in episodic lid mode the spectra are less smooth and drop off more rapidly with degree than Venus. In stagnant lid mode the amplitude of topography and geoid depend on reference viscosity; a reference viscosity in the range 3×10^{19} – 1×10^{20} Pa s (causing upper-mantle viscosities in the same range) produces Venus-like amplitudes and is consistent with a dry olivine rheology. In episodic lid mode, the topography and geoid are almost independent of reference viscosity. The viscosity profile assumed here, which is Earth-like but shifted to higher values, is capable of producing the observed admittance ratios, as also found by [Pauer *et al.*, 2006; Simons *et al.*, 1997]. However, model geoid and admittance ratios are far from a perfect fit to Venus so more investigation is warranted, including the effect of different viscosity profiles.

[86] 7. The basalt density inversion below 730 km [Ringwood, 1991] causes substantial compositional stratification around 730 km depth as in Ogawa [2000], and breakdown of this layering causes a significant increase in episodicity compared to cases in which it is not included, but its effect is far smaller than episodic lid overturn induced by plastic yielding.

[87] 8. The classical stagnant lid mode in which the interior temperature adjusts to be about a rheological temperature scale lower than the CMB temperature [e.g., Moresi and Solomatov, 1995; Jellinek *et al.* 2002], is not reached if, as seems likely for both Earth and Venus, the core starts superheated relative to the mantle [Stevenson, 1990]. Instead, the interior temperature is regulated by magmatism, while the core cools relatively slowly—slower than Earth's core due to the absence of subducted slabs reaching it. This results in hot plumes existing throughout Venus's history. Even so, the contribution of plumes to the surface heat flow is much lower than that due to radiogenic heating.

[88] 9. Present-day core heat flow is predicted to be in the range 4–10 TW for stagnant lid cases but 3 TW for episodic lid cases because the core becomes surrounded by a layer of subducted crust. The first may be similar to Earth [Lay *et al.*, 2008], but the episodic-lid value might be lower than that conducted down the core adiabat and therefore insufficient for a dynamo to exist. Earlier on it was much higher (e.g., 30 TW) for both tectonic modes, so a transition from dynamo to no dynamo seems likely, particularly in the episodic mode.

[89] The overall conclusion is that episodic lithospheric overturn provides the most straightforward way of simultaneously matching surface observations regarding resurfacing, topography, geoid, inferred crustal thickness and lack of dynamo. However, there are a number of model simplifications, the effect of which needs to be examined in the future. (1) 2-D geometry. While our preliminary 3-D spherical results display behavior that is similar to the presented spherical annulus results, they will allow a more detailed comparison of model surface features and deformation with surface features observed on Venus. They also obtain a slightly (~15%) lower magmatic heat flux, presumably due to the different planform of plumes, but this is not enough to solve the heat budget

problem. (2) The assumption that all magma produced shallower than a certain depth produces extrusive volcanism is an end member; much of the magma may intrude instead, which would result in a warm, weak crust. (3) The present models assume a diffusion-creep rheology plus plastic yielding, whereas stresses in the lithosphere and shallow mantle may be high enough for dislocation creep to dominate; according to Noack *et al.* [2012] this might reduce the viscosity enough to allow substantial surface motion. (4) Here basalt is assumed to have the same rheology as the upper mantle; the influence of weaker basalt needs to be investigated as in previous regional models [Buck, 1992; Lenardic *et al.*, 1993, 1995]. (5) Plastic yielding is a gross parameterization of small-scale processes such as those involving grain-size evolution [Bercovici and Ricard, 2012; Foley *et al.*, 2012; Landuyt and Bercovici, 2009]. (6) A more complex compositional model might be required to explain surface features and topography; for example Kaula [1990] postulated that intracrustal differentiation leads to silicic cratons, also favored by Jull and Arkani-Hamed [1995], and supported by recent near-infrared emission images favoring a felsic composition of tessera material [Basilevsky *et al.*, 2012]. (7) Outgassing- and escape-related changes in climate (surface temperature) have been postulated to have an effect on tectonics [Anderson and Smrekar, 1999; Solomon *et al.*, 1999], which seems to be borne out by parameterized [Phillips *et al.*, 2001] and dynamical models [Landuyt and Bercovici, 2009; Lenardic *et al.*, 2008; Noack *et al.*, 2012]; we are also investigating coupled models. (8) Outgassing of radiogenic argon is often cited as an important constraint [Kaula, 1999] although with large uncertainties [Watson *et al.*, 2007], but is something that can be quantitatively address with convection models [Xie and Tackley, 2004b].

[90] **Acknowledgments.** We thank Takashi Nakagawa and Dave Stegman for help with geoid calculation implementation and testing, and Francis Nimmo and Masaki Ogawa for their helpful reviews that improved the manuscript.

References

- Anderson, F. S., and S. E. Smrekar (1999), Tectonic effects of climate change on Venus, *J. Geophys. Res.*, *104*(E12), 30,743–30,756, doi:10.1029/1999JE001082.
- Anderson, F. S., and S. E. Smrekar (2006), Global mapping of crustal and lithospheric thickness on Venus, *J. Geophys. Res.*, *111*, E08006, doi:10.1029/2004JE002395.
- Basilevsky, A. T., and J. W. Head (2007), Beta regio, Venus: Evidence for uplift, rifting, and volcanism due to a mantle plume, *Icarus*, *192*, 167–186, doi:10.1016/j.icarus.2007.07.007.
- Basilevsky, A. T., *et al.* (2012), Geologic interpretation of the near-infrared images of the surface taken by the Venus Monitoring Camera, Venus Express, *Icarus*, *217*(2), 434–450, doi:10.1016/j.icarus.2011.11.003.
- Bercovici, D., and Y. Ricard (2012), Mechanisms for the generation of plate tectonics by two-phase grain-damage and pinning, *Phys. Earth Planet. Inter.*, *202–203*, 27–55, doi:10.1016/j.pepi.2012.05.003.
- Bindschadler, D. L., G. Schubert, and W. M. Kaula (1990), Mantle flow tectonics and the origin of Ishtar Terra, Venus, *Geophys. Res. Lett.*, *17*(9), 1345–1348, doi:10.1029/GL017i009p01345.
- Bindschadler, D. L., G. Schubert, and W. M. Kaula (1992), Coldspots and hotspots: Global tectonics and mantle dynamics of Venus, *J. Geophys. Res.*, *97*(E8), 13,495–13,532, doi:10.1029/92JE01165.
- Bjornnes, E. E., V. L. Hansen, B. James, and J. B. Swenson (2012), Equilibrium resurfacing of Venus: Results from new Monte Carlo modeling and implications for Venus surface histories, *Icarus*, *217*(2), 451–461, doi:10.1016/j.icarus.2011.03.033.
- Breuer, D., and W. B. Moore (2007), Dynamics and thermal history of the terrestrial planets, the Moon, and Io, in *Treatise on Geophysics*, vol. 10, *Planets and Moons*, edited by T. Spohn, pp. 299–348, Elsevier, Amsterdam, doi:10.1016/B978-044452748-6.00161-9.

- Brown, C. D., and R. E. Grimm (1999), Recent tectonic and lithospheric thermal evolution of Venus, *Icarus*, 139, 40–48, doi:10.1006/icar.1999.6083.
- Buck, W. R. (1992), Global decoupling of crust and mantle: Implications for topography, geoid and mantle viscosity on Venus, *Geophys. Res. Lett.*, 19(21), 2111–2114, doi:10.1029/92GL02462.
- Buffett, B. A., H. E. Huppert, J. R. Lister, and A. W. Woods (1992), Analytical model for solidification of the Earth's core, *Nature*, 356(6367), 329–331, doi:10.1038/356329a0.
- Buffett, B. A., H. E. Huppert, J. R. Lister, and A. W. Woods (1996), On the thermal evolution of the Earth's core, *J. Geophys. Res.*, 101(B4), 7989–8006, doi:10.1029/95JB03539.
- Bullock, M. A., and D. H. Grinspoon (2001), The recent evolution of climate on Venus, *Icarus*, 150(1), 19–37, doi:10.1006/icar.2000.6570.
- Carr, M. H., A. S. McEwen, K. A. Howard, F. C. Chuang, P. Thomas, P. Schuster, J. Oberst, G. Neukum, and G. Schubert (1998), Mountains and calderas on Io: Possible implications for lithosphere structure and magma generation, *Icarus*, 135(1), 146–165, doi:10.1006/icar.1998.5979.
- Christensen, U. R., and A. W. Hofmann (1994), Segregation of subducted oceanic crust in the convecting mantle, *J. Geophys. Res.*, 99(B10), 19,867–19,884, doi:10.1029/93JB03403.
- Christensen, U. R., and D. A. Yuen (1985), Layered convection induced by phase transitions, *J. Geophys. Res.*, 90(B12), 10,291–10,300, doi:10.1029/JB090iB12p10291.
- Davies, G. F. (1990), Heat and mass transport in the early Earth, in *Origin of the Earth*, edited by H. E. Newsome and J. H. Jones, pp. 175–194, Oxford Univ. Press, New York.
- Davies, G. F. (2006), Depletion of the early Earth's upper mantle and the viability of early plate tectonics, *Earth Planet. Sci. Lett.*, 243, 376–382, doi:10.1016/j.epsl.2006.01.053.
- Dombard, A. J., C. L. Johnson, M. A. Richards, and S. C. Solomon (2007), A magmatic loading model for coronae on Venus, *J. Geophys. Res.*, 112, E04006, doi:10.1029/2006JE002731.
- Dupeyrat, L., and C. Sotin (1995), The effect of the transformation of basalt to eclogite on the internal dynamics of Venus, *Planet. Space Sci.*, 43(7), 909–921, doi:10.1016/0032-0633(94)00227-1.
- Fegley, B., and R. G. Prinn (1989), Estimation of the rate of volcanism on Venus from reaction rate measurements, *Nature*, 337(6202), 55–58, doi:10.1038/337055a0.
- Fleitout, L., A. Mambole, and U. Christensen (2000), Phase changes around 670 km depth and segregation in the Earth's mantle, *Eos Trans. AGU*, 81(48), Fall Meeting Suppl., Abstract T12E-11.
- Foley, B. J., D. Bercovici, and W. Landuyt (2012), The conditions for plate tectonics on super-Earths: Inferences from convection models with damage, *Earth Planet. Sci. Lett.*, 331–332, 281–290, doi:10.1016/j.epsl.2012.03.028.
- Fowler, A. C., and S. B. G. O'Brien (1996), A mechanism for episodic subduction on Venus, *J. Geophys. Res.*, 101(E2), 4755–4763, doi:10.1029/95JE03261.
- Fujita, K., and M. Ogawa (2009), Basaltic accumulation instability and chaotic plate motion in the earliest mantle inferred from numerical experiments, *J. Geophys. Res.*, 114, B10402, doi:10.1029/2008JB006222.
- Golle, O., C. Dumoulin, G. Choblet, and O. Cadek (2012), Topography and geoid induced by a convecting mantle beneath an elastic lithosphere, *Geophys. J. Int.*, 189(1), 55–72, doi:10.1111/j.1365-246X.2012.05364.x.
- Grimm, R. E. (1994a), Recent deformation rates on Venus, *J. Geophys. Res.*, 99(E11), 23,163–23,171, doi:10.1029/94JE02196.
- Grimm, R. E. (1994b), The deep structure of Venusian plateau highlands, *Icarus*, 112(1), 89–103, doi:10.1006/icar.1994.1171.
- Guest, J. E., and E. R. Stofan (1999), A new view of the stratigraphic history of Venus, *Icarus*, 139, 55–66, doi:10.1006/icar.1999.6091.
- Hauck, S. A., II, R. J. Phillips, and M. H. Price (1998), Venus: Crater distribution and plains resurfacing models, *J. Geophys. Res.*, 103(E6), 13,635–13,642, doi:10.1029/98JE00400.
- Hernlund, J. W., and P. Tackley (2008), Modeling mantle convection in the spherical annulus, *Phys. Earth Planet. Inter.*, 171(1–4), 48–54, doi:10.1016/j.pepi.2008.07.037.
- Herrick, R. R. (1994), Resurfacing history of Venus, *Geology*, 22(8), 703–706, doi:10.1130/0091-7613(1994)022<0703:RHOV>2.3.CO;2.
- Herrick, R. R. (1999), Small mantle upwellings are pervasive on Venus and Earth, *Geophys. Res. Lett.*, 26(6), 803–806, doi:10.1029/1999GL900063.
- Hirose, K., N. Takafuji, N. Sata, and Y. Ohishi (2005), Phase transition and density of subducted MORB crust in the lower mantle, *Earth Planet. Sci. Lett.*, 237, 239–251, doi:10.1016/j.epsl.2005.06.035.
- Hoogenboom, T., and G. A. Houseman (2006), Rayleigh-Taylor instability as a mechanism for corona formation on Venus, *Icarus*, 180, 292–307, doi:10.1016/j.icarus.2005.11.001.
- Irifune, T., and A. E. Ringwood (1993), Phase-transformations in subducted oceanic crust and buoyancy relationships at depths of 600–800 km in the mantle, *Earth Planet. Sci. Lett.*, 117(1–2), 101–110, doi:10.1016/0012-821X(93)90120-X.
- Janes, D. M., S. W. Squyres, D. L. Bindschadler, G. Baer, G. Schubert, V. L. Sharpton, and E. R. Stofan (1992), Geophysical models for the formation and evolution of coronae on Venus, *J. Geophys. Res.*, 97(E10), 16,055–16,067, doi:10.1029/92JE01689.
- Janle, P., A. T. Basilevsky, M. A. Kreslavsky, and E. N. Slyuta (1992), Heat loss and tectonic style of Venus, *Earth Moon Planets*, 58(1), 1–29, doi:10.1007/BF00058070.
- Jellinek, A. M., A. Lenardic, and M. Manga (2002), The influence of interior mantle temperature on the structure of plumes: Heads for Venus, tails for the Earth, *Geophys. Res. Lett.*, 29(11), 1532, doi:10.1029/2001GL014624.
- Johnson, C. L., and M. A. Richards (2003), A conceptual model for the relationship between coronae and large-scale mantle dynamics on Venus, *J. Geophys. Res.*, 108(E6), 5058, doi:10.1029/2002JE001962.
- Jull, M. G., and J. Arkani-Hamed (1995), The implications of basalt in the formation and evolution of mountains on Venus, *Phys. Earth Planet. Inter.*, 89, 163–175, doi:10.1016/0031-9201(95)03015-O.
- Karato, S., and P. Wu (1993), Rheology of the upper mantle: A synthesis, *Science*, 260(5109), 771–778, doi:10.1126/science.260.5109.771.
- Kaula, W. M. (1990), Mantle convection and crustal evolution on Venus, *Geophys. Res. Lett.*, 17(9), 1401–1403, doi:10.1029/GL017i009p01401.
- Kaula, W. M. (1999), Constraints on Venus evolution from radiogenic argon, *Icarus*, 139(1), 32–39, doi:10.1006/icar.1999.6082.
- Keller, T., and P. J. Tackley (2009), Towards self-consistent modelling of the Martian dichotomy: The influence of low-degree convection on crustal thickness distribution, *Icarus*, 202(2), 429–443, doi:10.1016/j.icarus.2009.03.029.
- Kiefer, W. S., and B. H. Hager (1991a), Mantle downwelling and crustal convergence: A model for Ishtar Terra, Venus, *J. Geophys. Res.*, 96(E4), 20,967–20,980, doi:10.1029/91JE02219.
- Kiefer, W. S., and B. H. Hager (1991b), A mantle plume model for the equatorial highlands of Venus, *J. Geophys. Res.*, 96(E4), 20,947–20,966, doi:10.1029/91JE02221.
- Kiefer, W. S., and B. H. Hager (1992), Geoid anomalies and dynamic topography from convection in cylindrical geometry: Applications to mantle plumes on Earth and Venus, *Geophys. J. Int.*, 108(1), 198–214, doi:10.1111/j.1365-246X.1992.tb00850.x.
- Kiefer, W. S., M. A. Richards, B. H. Hager, and B. G. Bills (1986), A dynamic model of Venus's gravity field, *Geophys. Res. Lett.*, 13(1), 14–17, doi:10.1029/GL013i001p00014.
- Kite, E. S., M. Manga, and E. Gaidos (2009), Geodynamics and rate of volcanism on massive Earth-like planets, *Astrophys. J.*, 700(2), 1732, doi:10.1088/0004-637X/700/2/1732.
- Koch, D. M., and M. Manga (1996), Neutrally buoyant diapirs: A model for Venus coronae, *Geophys. Res. Lett.*, 23(3), 225–228, doi:10.1029/95GL03776.
- Kohlstedt, D. L., B. Evans, and S. J. Mackwell (1995), Strength of the lithosphere: Constraints imposed by laboratory experiments, *J. Geophys. Res.*, 100(B9), 17,587–17,602, doi:10.1029/95JB01460.
- Konopliv, A. S., and W. L. Sjogren (1994), Venus spherical harmonic gravity model to degree and order 60, *Icarus*, 112(1), 42–54, doi:10.1006/icar.1994.1169.
- Konopliv, A. S., W. B. Banerdt, and W. L. Sjogren (1999), Venus gravity: 180th degree and order model, *Icarus*, 139, 3–18, doi:10.1006/icar.1999.6086.
- Kucinskas, A. B., and D. L. Turcotte (1994), Isostatic compensation of equatorial highlands on Venus, *Icarus*, 112, 104–116.
- Landuyt, W., and D. Bercovici (2009), Variations in planetary convection via the effect of climate on damage, *Earth Planet. Sci. Lett.*, 277, 29–37, doi:10.1016/j.epsl.2008.09.034.
- Lay, T., J. Hernlund, and B. A. Buffett (2008), Core-mantle boundary heat flow, *Nat. Geosci.*, 1(1), 25–32, doi:10.1038/ngeo.2007.44.
- Lenardic, A., W. M. Kaula, and D. L. Bindschadler (1991), The tectonic evolution of western Ishtar Terra, Venus, *Geophys. Res. Lett.*, 18(12), 2209–2212, doi:10.1029/91GL02734.
- Lenardic, A., W. M. Kaula, and D. L. Bindschadler (1993), A mechanism for crustal recycling on Venus, *J. Geophys. Res.*, 98(E10), 18,697–18,705, doi:10.1029/93JE01799.
- Lenardic, A., W. M. Kaula, and D. L. Bindschadler (1995), Some effects of a dry crustal flow law on numerical simulations of coupled crustal deformation and mantle convection on Venus, *J. Geophys. Res.*, 100(E8), 16,949–16,957, doi:10.1029/95JE01895.
- Lenardic, A., A. M. Jellinek, and L. N. Moresi (2008), A climate induced transition in the tectonic style of a terrestrial planet, *Earth Planet. Sci. Lett.*, 271(1–4), 34–42, doi:10.1016/j.epsl.2008.03.031.
- Loddoch, A., C. Stein, and U. Hansen (2006), Temporal variations in the convective style of planetary mantles, *Earth Planet. Sci. Lett.*, 251, 79–89, doi:10.1016/j.epsl.2006.08.026.
- Machel, P., and P. Weber (1991), Intermittent layered convection in a model mantle with an endothermic phase-change at 670 km, *Nature*, 350(6313), 55–57, doi:10.1038/350055a0.

- McKenzie, D. (1994), The relationship between topography and gravity on Earth and Venus, *Icarus*, *112*(1), 55–88, doi:10.1006/icar.1994.1170.
- McKenzie, D., and M. J. Bickle (1988), The volume and composition of melt generated by extension of the lithosphere, *J. Petrol.*, *29*(3), 625–679.
- McKenzie, D., P. G. Ford, C. Johnson, B. Parsons, D. Sandwell, S. Saunders, and S. C. Solomon (1992), Features on Venus generated by plate boundary processes, *J. Geophys. Res.*, *97*(E8), 13,533–13,544, doi:10.1029/92JE01350.
- Mitrovica, J. X., and A. M. Forte (2004), A new inference of mantle viscosity based upon joint inversion of convection and glacial isostatic adjustment data, *Earth Planet. Sci. Lett.*, *225*, 177–189, doi:10.1016/j.epsl.2004.06.005.
- Moore, W. B. (2001), The thermal state of Io, *Icarus*, *154*(2), 548–550, doi:10.1006/icar.2001.6739.
- Moore, W. B., and G. Schubert (1997), Venusian crustal and lithospheric properties from nonlinear regressions of highland geoid and topography, *Icarus*, *128*(2), 415–428, doi:10.1006/icar.1997.5750.
- Moore, W. B., and G. Schubert (1995), Lithospheric thickness and mantle/lithosphere density contrast beneath Beta Regio, Venus, *Geophys. Res. Lett.*, *22*(4), 429–432, doi:10.1029/94GL02055.
- Moresi, L., and B. Parsons (1995), Interpreting gravity, geoid, and topography for convection with temperature-dependent viscosity: Application to surface-features on Venus, *J. Geophys. Res.*, *100*(E10), 21,155–21,171, doi:10.1029/95JE01622.
- Moresi, L. N., and V. S. Solomatov (1995), Numerical investigation of 2D convection with extremely large viscosity variations, *Phys. Fluids*, *7*(9), 2154–2162, doi:10.1063/1.868465.
- Moresi, L., and V. Solomatov (1998), Mantle convection with a brittle lithosphere: Thoughts on the global tectonic styles of the Earth and Venus, *Geophys. J. Int.*, *133*(3), 669–682, doi:10.1046/j.1365-246X.1998.00521.x.
- Nakagawa, T., and B. A. Buffett (2005), Mass transport mechanism between the upper and lower mantle in numerical simulations of thermochemical mantle convection with multicomponent phase changes, *Earth Planet. Sci. Lett.*, *230*, 11–27, doi:10.1016/j.epsl.2004.11.005.
- Nakagawa, T., and P. J. Tackley (2004), Effects of thermo-chemical mantle convection on the thermal evolution of the Earth's core, *Earth Planet. Sci. Lett.*, *220*, 107–119, doi:10.1016/S0012-821X(04)00055-X.
- Nakagawa, T., and P. J. Tackley (2005a), Deep mantle heat flow and thermal evolution of the Earth's core in thermochemical multiphase models of mantle convection, *Geochem. Geophys. Geosyst.*, *6*, Q08003, doi:10.1029/2005GC000967.
- Nakagawa, T., and P. J. Tackley (2005b), The interaction between the post-perovskite phase change and a thermo-chemical boundary layer near the core-mantle boundary, *Earth Planet. Sci. Lett.*, *238*, 204–216, doi:10.1016/j.epsl.2005.06.048.
- Nakagawa, T., and P. J. Tackley (2010), Influence of initial CMB temperature and other parameters on the thermal evolution of Earth's core resulting from thermochemical spherical mantle convection, *Geochem. Geophys. Geosyst.*, *11*, Q06001, doi:10.1029/2010GC003031.
- Nakagawa, T., and P. J. Tackley (2012), Influence of magmatism on mantle cooling, surface heat flow and Urey ratio, *Earth Planet. Sci. Lett.*, *329*–*330*, 1–10, doi:10.1016/j.epsl.2012.02.011.
- Nakagawa, T., P. J. Tackley, F. Deschamps, and J. A. D. Connolly (2009), Incorporating self-consistently calculated mineral physics into thermochemical mantle convection simulations in a 3-D spherical shell and its influence on seismic anomalies in Earth's mantle, *Geochem. Geophys. Geosyst.*, *10*, Q03004, doi:10.1029/2008GC002280.
- Nakagawa, T., P. J. Tackley, F. Deschamps, and J. A. D. Connolly (2010), The influence of MORB and harzburgite composition on thermochemical mantle convection in a 3-D spherical shell with self-consistently calculated mineral physics, *Earth Planet. Sci. Lett.*, *296*, 403–412, doi:10.1016/j.epsl.2010.05.026.
- Namiki, N., and S. C. Solomon (1998), Volcanic degassing of argon and helium and the history of crustal production on Venus, *J. Geophys. Res.*, *103*(E2), 3655–3677, doi:10.1029/97JE03032.
- Nimmo, F., and D. McKenzie (1996), Modelling plume-related uplift, gravity and melting on Venus, *Earth Planet. Sci. Lett.*, *145*(1–4), 109–123, doi:10.1016/S0012-821X(96)00200-2.
- Nimmo, F., and D. P. McKenzie (1997), Convective thermal evolution of the upper mantles of Earth and Venus, *Geophys. Res. Lett.*, *24*(12), 1539–1543, doi:10.1029/97GL01382.
- Noack, L., D. Breuer, and T. Spohn (2012), Coupling the atmosphere with interior dynamics: Implications for the resurfacing of Venus, *Icarus*, *217*(2), 484–498, doi:10.1016/j.icarus.2011.08.026.
- Ogawa, M. (2000), Numerical models of magmatism in convecting mantle with temperature-dependent viscosity and their implications for Venus and Earth, *J. Geophys. Res.*, *105*(E3), 6997–7012, doi:10.1029/1999JE001162.
- Ogawa, M. (2007), Superplumes, plates, and mantle magmatism in two-dimensional numerical models, *J. Geophys. Res.*, *112*, B06404, doi:10.1029/2006JB004533.
- Ogawa, M., and H. Nakamura (1998), Thermochemical regime of the early mantle inferred from numerical models of the coupled magmatism-mantle convection system with the solid-solid phase transitions at depths around 660 km, *J. Geophys. Res.*, *103*(B6), 12,161–12,180, doi:10.1029/98JB00611.
- Ogawa, M., and T. Yanagisawa (2011), Numerical models of Martian mantle evolution induced by magmatism and solid-state convection beneath stagnant lithosphere, *J. Geophys. Res.*, *116*, E08008, doi:10.1029/2010JE003777.
- Ohta, K., K. Hirose, T. Lay, N. Sata, and Y. Ohishi (2008), Phase transitions in pyrolite and MORB at lowermost mantle conditions: Implications for a MORB-rich pile above the core-mantle boundary, *Earth Planet. Sci. Lett.*, *267*, 107–117, doi:10.1016/j.epsl.2007.11.037.
- O'Neill, C., A. Lenardic, A. M. Jellinek, and W. S. Kiefer (2007), Melt propagation and volcanism in mantle convection simulations, with applications for Martian volcanic and atmospheric evolution, *J. Geophys. Res.*, *112*, E07003, doi:10.1029/2006JE002799.
- Ono, S., E. Ito, and T. Katsura (2001), Mineralogy of subducted basaltic crust (MORB) from 25 to 37 GPa, and chemical heterogeneity of the lower mantle, *Earth Planet. Sci. Lett.*, *190*(1–2), 57–63, doi:10.1016/S0012-821X(01)00375-2.
- O'Reilly, T. C., and G. F. Davies (1981), Magma transport of heat on Io: A mechanism allowing a thick lithosphere, *Geophys. Res. Lett.*, *8*, 313–316, doi:10.1029/GL008i004p00313.
- Orth, C. P., and V. S. Solomatov (2011), The isostatic stagnant lid approximation and global variations in the Venusian lithospheric thickness, *Geochem. Geophys. Geosyst.*, *12*, Q07018, doi:10.1029/2011GC003582.
- Papuc, A. M., and G. F. Davies (2012), Transient mantle layering and the episodic behaviour of Venus due to the 'basalt barrier' mechanism, *Icarus*, *217*(2), 499–509, doi:10.1016/j.icarus.2011.09.024.
- Pauer, M., K. Fleming, and O. Cadek (2006), Modeling the dynamic component of the geoid and topography of Venus, *J. Geophys. Res.*, *111*, E11012, doi:10.1029/2005JE002511.
- Peltier, W. R., and R. Drummond (2010), Deepest mantle viscosity: Constraints from Earth rotation anomalies, *Geophys. Res. Lett.*, *37*, L12304, doi:10.1029/2010GL043219.
- Peltier, W. R., and L. P. Solheim (1992), Mantle phase-transitions and layered chaotic convection, *Geophys. Res. Lett.*, *19*(3), 321–324, doi:10.1029/91GL02951.
- Phillips, R. J., R. F. Raubertas, R. E. Arvidson, I. C. Sarkar, R. R. Herrick, N. Izenberg, and R. E. Grimm (1992), Impact craters and Venus resurfacing history, *J. Geophys. Res.*, *97*(E10), 15,923–15,948, doi:10.1029/92JE01696.
- Phillips, R. J., M. A. Bullock, and S. A. Hauck II (2001), Climate and interior coupled evolution on Venus, *Geophys. Res. Lett.*, *28*(9), 1779–1782, doi:10.1029/2000GL011821.
- Phipps Morgan, J. (1998), Thermal and rare gas evolution of the mantle, *Chem. Geol.*, *145*, 431–445, doi:10.1016/S0009-2541(97)00153-8.
- Pozzo, M., C. Davies, D. Gubbins, and D. Alfe (2012), Thermal and electrical conductivity of iron at Earth's core conditions, *Nature*, *485*(7398), 355–358, doi:10.1038/nature11031.
- Rappaport, N. J., A. S. Konopliv, and A. B. Kucinskis (1999), An improved 360 degree and order model of Venus topography, *Icarus*, *139*, 19–31, doi:10.1006/icar.1999.6081.
- Ratcliff, J. T., G. Schubert, and A. Zebib (1995), Three-dimensional variable viscosity convection of an infinite Prandtl Number Boussinesq fluid in a spherical shell, *Geophys. Res. Lett.*, *22*(16), 2227–2230, doi:10.1029/95GL00784.
- Ratcliff, J. T., P. J. Tackley, G. Schubert, and A. Zebib (1997), Transitions in thermal convection with strongly variable viscosity, *Phys. Earth Planet. Inter.*, *102*, 201–212, doi:10.1016/S0031-9201(97)00013-7.
- Reese, C. C., V. S. Solomatov, and L.-N. Moresi (1998), Heat transport efficiency for stagnant lid convection with dislocation viscosity: Application to Mars and Venus, *J. Geophys. Res.*, *103*(E6), 13,643–13,657, doi:10.1029/98JE01047.
- Reese, C. C., V. S. Solomatov, and L.-N. Moresi (1999), Non-Newtonian stagnant lid convection and magmatic resurfacing on Venus, *Icarus*, *139*(1), 67–80, doi:10.1006/icar.1999.6088.
- Reese, C. C., V. S. Solomatov, and C. P. Orth (2007), Mechanisms for cessation of magmatic resurfacing on Venus, *J. Geophys. Res.*, *112*, E04S04, doi:10.1029/2006JE002782.
- Ringwood, A. E. (1991), Phase-transformations and their bearing on the constitution and dynamics of the mantle, *Geochim. Cosmochim. Acta*, *55*(8), 2083–2110, doi:10.1016/0016-7037(91)90090-R.
- Sandwell, D. T., and G. Schubert (1992a), Flexural ridges, trenches, and outer rises around coronae on Venus, *J. Geophys. Res.*, *97*(E10), 16,069–16,083, doi:10.1029/92JE01274.
- Sandwell, D. T., and G. Schubert (1992b), Evidence for retrograde lithospheric subduction on Venus, *Science*, *257*(5071), 766–770, doi:10.1126/science.257.5071.766.

- Schaber, G. G., R. G. Strom, H. J. Moore, L. A. Soderblom, R. L. Kirk, D. J. Chadwick, D. D. Dawson, L. R. Gaddis, J. M. Boyce, and J. Russell (1992), Geology and distribution of impact craters on Venus: What are they telling us?, *J. Geophys. Res.*, 97(E8), 13,257–13,301, doi:10.1029/92JE01246.
- Schubert, G., and D. T. Sandwell (1995), A global survey of possible subduction sites on Venus, *Icarus*, 117, 173–196, doi:10.1006/icar.1995.1150.
- Schubert, G., D. Bercovici, and G. A. Glatzmaier (1990), Mantle dynamics in Mars and Venus: Influence of an immobile lithosphere on three-dimensional mantle convection, *J. Geophys. Res.*, 95(B9), 14,105–14,129, doi:10.1029/JB095iB09p14105.
- Schubert, G., D. L. Turcotte, V. Solomatov, and P. J. Tackley (1997), Mantle convection and the thermal evolution of Venus, in *Venus II: Geology, Geophysics, Atmosphere, and Solar Wind Environments*, edited by S. W. Bougher, D. M. Hunten, and R. J. Phillips, pp. 1245–1289, Univ. of Ariz. Press, Tucson.
- Simons, M., B. H. Hager, and S. C. Solomon (1994), Global variations in the geoid/topography admittance of Venus, *Science*, 264(5160), 798–803, doi:10.1126/science.264.5160.798.
- Simons, M., S. C. Solomon, and B. H. Hager (1997), Localization of gravity and topography: Constraints on the tectonics and mantle dynamics of Venus, *Geophys. J. Int.*, 131(1), 24–44, doi:10.1111/j.1365-246X.1997.tb00593.x.
- Smolarkiewicz, P. K. (1984), A fully multidimensional positive definite advection transport algorithm with small implicit diffusion, *J. Comput. Phys.*, 54(2), 325–362, doi:10.1016/0021-9991(84)90121-9.
- Smrekar, S. E., and E. M. Parmentier (1996), The interaction of mantle plumes with surface thermal and chemical boundary layers: Applications to hotspots on Venus, *J. Geophys. Res.*, 101(B3), 5397–5410, doi:10.1029/95JB02877.
- Smrekar, S. E., and E. R. Stofan (1999), Origin of corona-dominated topographic rises on Venus, *Icarus*, 139, 100–115, doi:10.1006/icar.1999.6090.
- Smrekar, S. E., E. R. Stofan, N. Mueller, A. Treiman, L. Elkins-Tanton, J. Helbert, G. Piccioni, and P. Drossart (2010), Recent hotspot volcanism on Venus from VIRTIS emissivity data, *Science*, 328(5978), 605–608, doi:10.1126/science.1186785.
- Solomatov, V. S., and L. N. Moresi (1996), Stagnant lid convection on Venus, *J. Geophys. Res.*, 101(E2), 4737–4753, doi:10.1029/95JE03361.
- Solomon, S. C., and J. W. Head (1982), Mechanisms for lithospheric heat transport on Venus: Implications for tectonic style and volcanism, *J. Geophys. Res.*, 87(B11), 9236–9246, doi:10.1029/JB087iB11p09236.
- Solomon, S. C., M. A. Bullock, and D. H. Grinspoon (1999), Climate change as a regulator of tectonics on Venus, *Science*, 286(5437), 87–90, doi:10.1126/science.286.5437.87.
- Spohn, T. (1991), Mantle differentiation and thermal evolution of Mars, Mercury, and Venus, *Icarus*, 90(2), 222–236, doi:10.1016/0019-1035(91)90103-Z.
- Stein, C., A. Fahl, and U. Hansen (2010), Resurfacing events on Venus: Implications on plume dynamics and surface topography, *Geophys. Res. Lett.*, 37, L01201, doi:10.1029/2009GL041073.
- Steinbach, V., and D. A. Yuen (1992), The effects of multiple phase-transitions on Venusian mantle convection, *Geophys. Res. Lett.*, 19(22), 2243–2246, doi:10.1029/92GL02319.
- Steinberger, B., and A. R. Calderwood (2006), Models of large-scale viscous flow in the Earth's mantle with constraints from mineral physics and surface observations, *Geophys. J. Int.*, 167(3), 1461–1481, doi:10.1111/j.1365-246X.2006.03131.x.
- Steinberger, B., S. C. Werner, and T. H. Torsvik (2010), Deep versus shallow origin of gravity anomalies, topography and volcanism on Earth, Venus and Mars, *Icarus*, 207(2), 564–577, doi:10.1016/j.icarus.2009.12.025.
- Stevenson, D. J. (1990), Fluid dynamics of core formation, in *Origin of the Earth*, edited by H. E. Newman and J. H. Jones, pp. 231–249, Oxford Univ. Press, Cambridge, UK.
- Stevenson, D. J., and S. C. McNamara (1988), Background heatflow on hotspot planets: Io and Venus, *Geophys. Res. Lett.*, 15(13), 1455–1458, doi:10.1029/GL015i013p01455.
- Stixrude, L., and C. Lithgow-Bertelloni (2011), Thermodynamics of mantle minerals: II. Phase equilibria, *Geophys. J. Int.*, 184, 1180–1213, doi:10.1111/j.1365-246X.2010.04890.x.
- Stoddard, P. R., and D. M. Jurdy (2012), Topographic comparisons of uplift features on Venus and Earth: Implications for Venus tectonics, *Icarus*, 217(2), 524–533, doi:10.1016/j.icarus.2011.09.003.
- Stofan, E. R., D. L. Bindschadler, J. W. Head, and E. M. Parmentier (1991), Corona structures on Venus: Models of origin, *J. Geophys. Res.*, 96(E4), 20,933–20,946, doi:10.1029/91JE02218.
- Stofan, E. R., S. E. Smrekar, D. L. Bindschadler, and D. A. Senske (1995), Large topographic rises on Venus: Implications for mantle upwelling, *J. Geophys. Res.*, 100(E11), 23,317–23,327, doi:10.1029/95JE01834.
- Stolper, E., D. Walker, B. H. Hager, and J. F. Hays (1981), Melt segregation from partially molten source regions: The importance of melt density and source region size, *J. Geophys. Res.*, 86(B7), 6261–6271, doi:10.1029/JB086iB07p06261.
- Strom, R. G., G. G. Schaber, and D. D. Dawson (1994), The global resurfacing of Venus, *J. Geophys. Res.*, 99(E5), 10,899–10,926, doi:10.1029/94JE00388.
- Sun, S.-S., and W. F. McDonough (1989), Chemical and isotopic systematics of oceanic basalts: Implications for mantle composition and processes, in *Magmatism in the Ocean Basins*, edited by A. D. Saunders and M. J. Norry, pp. 313–345, Geol. Soc. Spec. Publ., Oxford, U. K. doi:10.1144/GSL.SP.1989.042.01.19.
- Tackley, P. J. (1996), Effects of strongly variable viscosity on three-dimensional compressible convection in planetary mantles, *J. Geophys. Res.*, 101, 3311–3332, doi:10.1029/95JB03211.
- Tackley, P. J. (1998), Three-dimensional simulations of mantle convection with a thermo-chemical basal boundary layer: D"? in *The Core-Mantle Boundary Region*, *Geodyn. Ser.*, vol. 28, edited by M. Gurnis et al., pp. 231–253, AGU, Washington, D. C., doi:10.1029/GD028p0231.
- Tackley, P. J. (2000), Self-consistent generation of tectonic plates in time-dependent, three-dimensional mantle convection simulations, *Geochem. Geophys. Geosyst.*, 1(8), 1021, doi:10.1029/2000GC000036.
- Tackley, P. J. (2008), Modelling compressible mantle convection with large viscosity contrasts in a three-dimensional spherical shell using the yin-yang grid, *Phys. Earth Planet. Inter.*, 171, 7–18.
- Tackley, P. J. (2012), Dynamics and evolution of the deep mantle resulting from thermal, chemical, phase and melting effects, *Earth Sci. Rev.*, 110, 1–25, doi:10.1016/j.earscirev.2011.10.001.
- Tackley, P. J., and S. D. King (2003), Testing the tracer ratio method for modeling active compositional fields in mantle convection simulations, *Geochem. Geophys. Geosyst.*, 4, 8302, doi:10.1029/2001GC000214.
- Tackley, P. J., D. J. Stevenson, G. A. Glatzmaier, and G. Schubert (1993), Effects of an endothermic phase transition at 670 km depth in a spherical model of convection in the Earth's mantle, *Nature*, 361(6414), 699–704, doi:10.1038/361699a0.
- Tackley, P. J., S. Xie, T. Nakagawa, and J. W. Hernlund (2005), Numerical and laboratory studies of mantle convection: Philosophy, accomplishments and thermochemical structure and evolution, in *Earth's Deep Mantle: Structure, Composition and Evolution*, *Geophys. Monogr. Ser.*, vol. 160, edited by R. D. van der Hilst et al., pp. 83–99, AGU, Washington, D. C., doi:10.1029/160GM07.
- Trompert, R., and U. Hansen (1998), Mantle convection simulations with rheologies that generate plate-like behavior, *Nature*, 395(6703), 686–689, doi:10.1038/27185.
- Turcotte, D. L. (1993), An episodic hypothesis for Venusian tectonics, *J. Geophys. Res.*, 98(E9), 17,061–17,068, doi:10.1029/93JE01775.
- Turcotte, D. L. (1995), How does Venus lose heat?, *J. Geophys. Res.*, 100(E8), 16,931–16,940, doi:10.1029/95JE01621.
- van Heck, H., and P. J. Tackley (2008), Planforms of self-consistently generated plate tectonics in 3-D spherical geometry, *Geophys. Res. Lett.*, 35, L19312, doi:10.1029/2008GL035190.
- van Thienen, P., N. J. Vlaar, and A. P. van den Berg (2005), Assessment of the cooling capacity of plate tectonics and flood volcanism in the evolution of Earth, Mars and Venus, *Phys. Earth Planet. Inter.*, 150, 287–315, doi:10.1016/j.pepi.2004.11.010.
- Vezolainen, A., V. S. Solomatov, J. W. Head, A. T. Basilevsky, and L.-N. Moresi (2003), Timing of formation of Beta Regio and its geodynamic implications, *J. Geophys. Res.*, 108(E1), 5002, doi:10.1029/2002JE001889.
- Watson, E. B., J. B. Thomas, and D. J. Cherniak (2007), ⁴⁰Ar retention in the terrestrial planets, *Nature*, 449, 299–304, doi:10.1038/nature06144.
- Weinstein, S. A. (1996), The potential role of non-Newtonian rheology in the resurfacing of Venus, *Geophys. Res. Lett.*, 23(5), 511–514, doi:10.1029/96GL00387.
- Wieczorek, M. A. (2007), Gravity and topography of the terrestrial planets, in *Treatise on Geophysics*, vol. 10, *Planets and Moons*, edited by T. Spohn, pp. 165–206, Elsevier, Amsterdam.
- Xie, S., and P. J. Tackley (2004a), Evolution of U-Pb and Sm-Nd systems in numerical models of mantle convection, *J. Geophys. Res.*, 109, B11204, doi:10.1029/2004JB003176.
- Xie, S., and P. J. Tackley (2004b), Evolution of helium and argon isotopes in a convecting mantle, *Phys. Earth Planet. Inter.*, 146(3–4), 417–439, doi:10.1016/j.pepi.2004.04.003.
- Xu, W., C. Lithgow-Bertelloni, L. Stixrude, and J. Ritsema (2008), The effect of bulk composition on mantle seismic structure, *Earth Planet. Sci. Lett.*, 275, 70–79, doi:10.1016/j.epsl.2008.08.012.
- Yamazaki, D., and S. Karato (2001), Some mineral physics constraints on the rheology and geothermal structure of Earth's lower mantle, *Am. Mineral.*, 86(4), 385–391.

- Yuen, D. A., D. M. Reuteler, S. Balachandar, V. Steinbach, A. V. Malevsky, and J. J. Smedsmo (1994), Various influences on 3-dimensional mantle convection with phase-transitions, *Phys. Earth Planet. Inter.*, *86*(1–3), 185–203, doi:10.1016/0031-9201(94)05068-6.
- Zhang, S. X., and U. Christensen (1993), Some effects of lateral viscosity variations on geoid and surface velocities induced by density anomalies in the mantle, *Geophys. J. Int.*, *114*(3), 531–547, doi:10.1111/j.1365-246X.1993.tb06985.x.
- Zhong, S., A. K. McNamara, E. Tan, L. Moresi, and M. Gurnis (2008), A benchmark study on mantle convection in a 3-D spherical shell using CitcomS, *Geochem. Geophys. Geosyst.*, *9*, Q10017, doi:10.1029/2008GC002048.